2008

Cooking up quantum chemistry

Bosiljka Njegic
Iowa State University

Cooking up quantum chemistry

by

Bosiljka Njegic

A dissertation submitted to the graduate faculty

in partial fulfillment of the requirements for the degree of

DOCTOR OF PHILOSOPHY

Major: Chemistry

Program of Study Committee:
Mark Gordon, Major Professor
Amy Andreotti
Gordon Miller
Hans Stauffer
Jim Evans

Iowa State University

Ames, Iowa

2008

TABLE OF CONTENTS

ACKNOWLEDGMENTS

"Anybody who has been seriously engaged in scientific work of any kind realizes that over the entrance to the gates of the temple of science are written the words: 'Ye must have faith.' " - Max Planck (1858-1947)

The path of a graduate student is convoluted and perilous. I joined Mark Gordon's group in my second year of graduate school. I was groomed to be an inorganic chemist at that point. My experience with quantum chemistry was at best limited and insofar as programming went, yes, I new of the existence of DO loops and IF statements. To my great surprise, Mark accepted me without questioning and led me gradually into the world of theoretical chemistry and computer programming. I can honestly say that Mark's motto is:

"Anyone can learn quantum chemistry."

I remember choosing my first projects not more then two months into joining his research group. We were talking in his office and he was laying out for me all the projects that I could possibly work on. I was and I still am inorganic chemist at heart, when he mentioned a reaction that is catalyzed by gold nanoparticles, I immediately jumped on it. It seemed natural to me to work on the mechanism of the reaction where gold exhibits peculiar chemical reactivity. However I still remember the words of caution from Mark, that this was quite a difficult project in spite of involving only 7 atoms, which I naively thought it would be very easy to handle due to its small size.

How mistaken I was! Nevertheless, Mark stood by my side in years to come and through failures, frustrations and successes and we did see this project through.

I can never thank enough Mark for everything he has done for me. I traveled the world while being in his group. I met so many people whom I knew previously only by reading the papers they wrote. List of great scientific minds that I had opportunity to talk to or listen their research presentations is long. All of these experiences shaped me into who I am today as a scientist.

Finally, I grew as a person under Mark's influence. I hope our friendship will keep growing over years to come. Mark, thank you for everything form the bottom of my heart!

There are many people to whom I owe gratitude as well. I will name some of them who made professionally great impact on me: Prof. Takako Kudo, Prof. Benny Gerber, Prof. Evan Bieske, Prof. Michael Duncan, and Dr. Mike Schmidt. This list is by no means complete and it continues over all current and former members of the Gordon's research group.

I would also like to extend my thanks to my family and friends. My grandma, dad, mom, step mom, brother, Karolina, Uros, Adu (who is the newest addition to my family ☺), Lyuda, Sean, Ivana, Jelena, Abhi, Vasu, Filip and many others. Last but not least to the start of it all - the Big Bang, which made the universe such an interesting place to study!

CHAPTER 1. GENERAL INTRODUCTION

"A little learning is a dangerous thing, but we must take that risk because a little is as much as our biggest heads can hold." - George Bernard Shaw (1856-1950)

History of Chemistry

The origin of chemistry can be traced to the discovery of fire and its very first use for cooking at the dawn of the human race more than 200,000 years ago[1]. Many years passed before more sophisticated usage of fire was achieved by transforming clay into pottery some 30,000 years ago[2]. Some of the most important applications of chemistry that gave birth to modern human civilization came with the discovery of glass and metallurgy more then 5,000 years ago[3]. The first rational thoughts about the nature of all things came to be some 2,000 years ago. Two cultures above all, Greek and Arab, made the greatest impact, for better or worse, on scientific thought for many centuries to come. The Greek thought heritage culminated in the life's work[4] of Aristotle (384-323 B.C.). While on one hand, Aristotle provided a framework of ideas, which influenced and unified the scientific thought process throughout the world, much of the work in the following 2000 years was guided and in a certain way shadowed by Aristotle's ideas, with a constant need to reinforce or modify Aristotle's theories rather than develop completely new ones.

Another influential person in this early period in the history of chemistry is Abu Musa Jãbir ibn Hayyãn (721-815), to whom much of the contributions from the Arab part of the world are assigned[5]. One of the most important advancements during this

time was the introduction of experimental methods such as crystallization and distillation.

Gradually through the span of the ages, modern chemistry finally emerged with the work of Antoine Laurent Lavoisier (1743-1794). Lavoisier put great emphasis on exact scientific studies, introduced the systematic chemical nomenclature and expressed the law of conservation of matter by using very first modern chemical equation[6]:

" must of grapes = carbonic acid + alcohol "

The reign of experimental chemistry that started with Lavoisier has continued until today, although theoretical chemistry started making its way into the mainstream thought in the 19th century. At first, the exploitation of mathematics to study problems in chemistry was met with a great deal of resistance:

"Every attempt to employ mathematical methods in the study of chemical questions must be considered profoundly irrational and contrary to the spirit of chemistry.... if mathematical analysis should ever hold a prominent place in chemistry -- an aberration which is happily almost impossible -- it would occasion a rapid and widespread degeneration of that science." - Auguste Comte (1798-1857)

However, the series of experiments that followed shook the foundations of then current views. The battle over the true nature of light started raging in the 17th century. Two opposite positions were taken. Christiaan Huygens (1629–1695) thought that light exhibits a wave behavior[7], while Isaac Newton (1643-1727) claimed that light consists of particles[8]. In 1803 the wave nature of light was demonstrated by Young's double-slit experiment[7] (Thomas Young (1773-1829)).

However, Albert Einstein (1879-1955) showed in 1905 that photons have to be treated as particles[9] in order to explain the photoelectric experiment. Soon after, in 1927, the wave properties of electrons were demonstrated in the Davisson-Germer electron diffraction experiment[10]. All these and many other experiments conducted in the years around the turn of the 20th century raised an important question of the very nature of light and matter. These experiments offered contradictory answers, some recognizing wave behavior, some particle behavior. Out of the inability of classical mechanics to explanation these experimental findings, the new concept of wave-particle duality emerged and the field of quantum chemistry was born. The mathematical description in the form of the Schrödinger equation (SE),[11] by Erwin Rudolf Josef Alexander Schrödinger (1887-1961), and a rigorous mathematical formulation[12] by Paul Dirac (1902-1984), gave rise to modern quantum chemistry.

Modern Quantum Chemistry

Although mathematical understanding of quantum chemistry came very early its applications were very limited as Dirac pointed out:

"The underlying physical laws necessary for the mathematical theory of a large part of physics and the whole of chemistry are thus completely known, and the difficulty is only that the exact application of these laws leads to equations much too complicated to be soluble. It therefore becomes desirable that approximate practical methods of applying quantum mechanics should be developed, which can lead to an explanation of the main features of complex atomic systems without too much computation. Hence the quantum mechanical methods developed in the 1930s and

1940s are often referred to as theoretical molecular or atomic physics to underline the fact that they were more the application of quantum mechanics to chemistry and spectroscopy than answers to chemically relevant questions." - Paul Dirac.

Although the SE is relativistic and time dependent in its full form, the chemistry problems that were dealt with in this thesis allowed the use of a simplified version of the SE, which is non-relativistic and time-independent. Thus, the SE can be written as:

$$\hat{\mathrm{H}}|\Psi\rangle = E|\Psi\rangle \qquad \text{Eq. 1}$$

where $\hat{\mathrm{H}}$ is the operator, which operates on the wave function Ψ to yield the total energy of the system, E.

The SE can be solved analytically only for hydrogen and hydrogen-like atoms. There is a big gap to be bridged between calculations done on the hydrogen atom and being able to carry out calculations on complex systems involving large numbers of atoms and molecules. Thus, only by introducing approximations can one enable calculations involving many nuclei and electrons.

The Hamiltonian operator can be written in atomic units for N electrons and M nuclei as:

$$\hat{\mathrm{H}} = -\sum_{i=1}^{N}\frac{1}{2}\nabla_i^2 - \sum_{A=1}^{M}\frac{1}{2M_A}\nabla_A^2 - \sum_{i=1}^{N}\sum_{A=1}^{M}\frac{Z_A}{r_{iA}} + \sum_{i=1}^{N}\sum_{j>i}^{N}\frac{1}{r_{ij}} + \sum_{A=1}^{M}\sum_{B>A}^{M}\frac{Z_A Z_B}{R_{AB}} \qquad \text{Eq. 2}$$

where the terms are given as the operators of: kinetic energy of electrons (1st term), kinetic energy of nuclei (2nd term), attractive potential energy between electrons and nuclei (3rd term), repulsive potential energy of electrons (4th term) and repulsive potential energy of nuclei (5th term).

The problem can be simplified by recognizing that the motion of electrons and nuclei is separable due to the much higher mass of nuclei compared to the mass of electrons. In other words, the positions of electrons are instantaneously readjusted with respect to the positions of nuclei. This is known as the Born-Oppenheimer approximation[13], which leads a form of the SE that is parametrically dependent on the positions of the nuclei. Consequently, the 2nd term in Eq. 2 becomes zero and the 5th term becomes a constant, leaving the electronic SE to be solved for fixed positions of the nuclei. Upon obtaining the electronic energy, the total energy of the system can be computed by adding the nuclear-nuclear repulsion energy term.

Even this simplified SE is not solvable without the introduction of further approximations, since it still embodies the many-body problem. In order to reduce the SE to a one-electron problem, the Hartree-Fock approximation[14-17] is introduced, which treats the electron-electron repulsion in an average manner. Since the field, which each electron feels, depends on all the other electrons, the iterative procedure, the so-called self-consistent field method, has to be implemented to solve the Hartee-Fock (HF) equations.

Another important question regarding solving the SE via the HF approximation is a wave function. In many electron systems, the wave function can be expressed as a product of single electron wave functions called orbitals, each having spatial and spin parts. The spatial part of the one-electron wave function is expanded in a set of basis functions. Such a many electron wave function is known as Hartree product[14-16]. However, Hartree product does not fulfill an additional

requirement, Pauli exclusion principle, which imposes antisymmetry on the wave function[18]:

"A many electron wave function must be antisymmetric with respect to the interchange of the coordinate x (both space and spin) of any two electrons."

The antisymmetry (Pauli) principle, can be easily forced onto the wave function by using Slater determinants[19,20] as an elegant way of introducing the linear combination of Hartree product one-electron wave functions.

To summarize, Hartree-Fock is a variational method based on a single Slater determinant for closed shell systems, expressed in a set of basis functions. The larger and more complete the set of basis functions the lower will be the expectation value of the calculated energy. Although the reaching the complete (infinite) basis set is computationally not possible, there are techniques developed to extrapolate the calculated energy to the complete (infinite) basis set value[21].

Depending on the existence of unpaired electrons in the system different flavors of HF have to be used. Systems with all paired electrons can be treated by the restricted closed shell HF method[22]. However, if unpaired electrons are present, restricted open shell[23-28] or unrestricted[29] HF must be used. In restricted open and closed shell HF, the same spatial orbital is assigned to each pair of electrons. This usually leads to improper breaking of bonds due to the inherent inflexibility of the spin orbitals. By pulling an electron pair apart there is no way for these two electrons to be split into two spatial orbitals since they are forced to share the same orbital. On the other hand, in unrestricted HF every electron has its own spatial orbital, thus enabling correct bond breaking. Furthermore, since HF is a variational

method, by expanding the wave function over twice as many orbitals compared to restricted HF, the calculated energy will be closer to the exact value. However, unrestricted HF is not a proper spin eigenfunction, so it suffers from spin contamination, due to the mixing of different spin states.

Although the Hartree-Fock method does account for the correlation of electrons with parallel spin, the electrons with opposite spins are not correlated. Thus, Hartree-Fock is a computationally inexpensive method that has become a corner stone of electronic structure calculations. From this point on, further approximations can be introduced leading to various semi-empirical methods. Alternatively, more accurate *ab initio* methods can be developed by recovering the previously neglected electron correlation.

There are three *ab initio* paths that can be taken to improve the Hartree-Fock method: configuration interaction, perturbation theory or coupled cluster methods.

Configuration interaction (CI) is a variational method, which employs the linear combination of Slater determinants. While Hartree-Fock takes into consideration only the ground state configuration that is expressed by a single Slater determinant, CI accounts for all the possible electron excitations within the finite set of basis functions. In principle, the CI calculation performed with the complete basis set will yield the exact energy of the system. However this calculation is exceedingly demanding. Even if the complete basis set could be used, the CI method itself is computationally so expensive that it is feasible only for very small molecules. There are two approaches to lower the computational cost and still recover some dynamic correlation in the system. One is to the truncate the CI expansion to a certain level of

excitation, such as considering only singly and doubly excited determinants. Another approach would be to limit the number of orbitals that are used in the CI expansion to those that are of the utmost importance for the proper answering of the chemistry question at hand. This leads to the multiconfigurational self-consistent field method[30-32] (MCSCF), which splits the molecular orbitals into an active and an inactive space. The full CI is then performed within the active space neglecting any dynamic correlation that arises within the inactive space or between the active and the inactive spaces. However this method gets computationally very expensive quickly as the size of the active space is expanded. Approaches like occupation restricted multiple active space method[33] (ORMAS), were developed to tackle this issue by partitioning the active space into subspaces.

The MP[34] method is based on recovering the dynamic correlation by treating it as perturbation with respect to the Hartree-Fock Hamiltonian. The sum of 0^{th} and 1^{st} order energies are accounted for by the HF energy. If the system of interest is an open shell with unpaired electrons, then restricted open shell based perturbation theory may be used. There are several different implementations of restricted open shell perturbation theory of which the Z-averaged perturbation theory method[35,36] (ZAPT) is spin correct to second order. The ZAPT method treats the occupied molecular orbitals in the same way as in traditional restricted Hartree-Fock method. However, a singly occupied spin orbital is given as a linear combination of α and β spins:

$$\sigma^{+} = \frac{1}{\sqrt{2}}(\alpha + \beta) \qquad \text{Eq. 3}$$

$$\sigma^{-} = \frac{1}{\sqrt{2}}(\alpha - \beta) \qquad \text{Eq. 4}$$

Where σ^{+} is by convention assigned to the occupied and σ^{-} to the unoccupied spin orbital.

The coupled cluster method[37,38] is based on the wave function given in the exponential form:

$$\Psi = e^{T}\Phi_0 \qquad \text{Eq. 5}$$

where the exponential operator (e^{T}) is expanded as:

$$e^{T} = 1 + T + \frac{1}{2}T^{2} + \frac{1}{6}T^{3} + \ldots = \sum_{k=0}^{\infty}\frac{1}{k!}T^{k} \qquad \text{Eq. 6}$$

The cluster operator (T_i), upon acting on the HF reference wave function, generates all the i^{th} excitations. Thus by generally applying a non-truncated cluster operator as expressed in Eq. 6, the full CI energy would be recovered. However as this is computationally not feasible, the expansion of the cluster operator is truncated usually at double excitations ($T=T_1+T_2$) leading to the coupled cluster with singles and doubles (CCSD) method[39,40]. The approximate non-iterative triples are relatively inexpensive to compute and give rise to the CCSD(T) method[40,41]. This method is still quite expensive and is usually used to calculate single point energies at structures obtained at some lower level of theory such as MP2. New flavors of the coupled cluster methods have been developed in order to further improve accuracy without a significant increase in the computational cost, such as CR-CC(2,3) (CCL) method[42].

As mentioned earlier, all of these post-HF methods are used to solve the electronic SE constructed within the Born-Openheimer approximation, which fixes the positions of the nuclei. If the electronic SE is solved for many different positions of the nuclei, a potential energy surface (PES) is generated. The PES contains information about both chemical properties. However, generating the PES is computationally extremely expensive. Many efforts have been made to design faster, more accurate, and parallel codes to enable calculations on larger systems such as proteins, DNA molecules or solvated systems.

The universe as we know it is shaped and governed from within, at the quantum level, by forces and laws that still elude our reasoning and provoke our imagination. This quantum world is truly a magical realm that defies our intuition, and it is bringing together various branches of science, in a joint effort to discover its secrets. Although our knowledge has grown much since the first mathematical equations were laid down, there still remains much that needs to be understood. As the boundaries of the theoretical sciences are blurred and ease and speed of sharing information increases, it is evident that only through a unified effort, is there hope for the true nature of universe to be revealed.

Thesis Organization

This thesis is organized in the following manner. Chapters 2 and 3 are concerned with calculating accurate vibrational frequencies using the vibrational self-consistent field method (VSCF). The main focus of Chapter 2 is to explore the effect of anharmonicity of calculated frequencies on thermodynamic properties, such as

entropy. Although some VSCF method developments are presented in Chapter 2, these and other improvements in the manner in which a PES is generated in the VSCF method are discussed in greater detail in Chapter 3. The comparison of harmonic, scaled harmonic and anharmonic frequencies, was made. Furthermore, the computing of a PES within the VSCF method was coarse-grain parallelized in order to enable calculations on bigger molecules. The work conducted on the reaction mechanism of the industrially important process of production of H_2O_2 catalyzed by gold nanoparticles is presented in Chapter 4. General conclusions are presented in Chapter 5.

References

(1) McDougall, I.; Brown Francis, H.; Fleagle John, G. *Nature* **2005**, *433*, 733.

(2) Vandiver, P. B.; Sofer, O.; Klima, B.; Svoboda, J. *Science (Washington, DC, United States)* **1989**, *246*, 1002.

(3) Slawson, H. H. *Glass Industry* **1935**, *16*, 151.

(4) Aristotle *Meteorologica*; Harvard University Press: Cambridge,, 1962.

(5) Kraus, P. *Isis* **1931**, *15*, 7.

(6) Lavoisier, A. L. *Traitâe âelâementaire de chimie, prâesentâe dans un ordre nouveau et d'apráes les dâecouvertes modernes; avec figures*; Cuchet: Paris,, 1789.

(7) Crew, H.; Huygens, C.; Young, T.; Fresnel, A. J.; Arago, F. *The wave theory of light; memoirs of Huygens, Young and Fresnel*; American Book Company: New York, Cincinnati, 1900.

(8) Newton, I. Opticks, or, A treatise of the reflexions, refractions, inflexions and colours of light also two treatises of the species and magnitude of curvilinear figures; Printed for S. Smith and B. Walford,: London, 1704.

(9) Einstein, A. *Annalen der Physik (Weinheim, Germany)* **1905**, *17*, 132.

(10) Davisson, C.; Germer, L. H. *Physical Review* **1927**, *30*, 705.

(11) Schrodinger, E. *Physical Review* **1926**, *28*, 1049.

(12) Dirac, P. A. M. *The principles of quantum mechanics*; The Clarendon Press: Oxford,, 1930.

(13) Born, M.; Oppenheimer, R. *Annalen der Physik (Berlin, Germany)* **1927**, *84*, 457.

(14) Hartree, D. R. *Proc. Cambridge Phil. Soc.* **1928**, *24*, 89.

(15) Hartree, D. R. *Proc. Cambridge Phil. Soc.* **1928**, *24*, 111.

(16) Hartree, D. R. *Proc. Cambridge Phil. Soc.* **1928**, *24*, 426.

(17) Fock, V. *Zeitschrift fuer Physik* **1930**, *62*, 795.

(18) Szabo, A.; Ostlund, N. S. *Modern quantum chemistry : introduction to advanced electronic structure theory*, 1st. ed.; McGraw-Hill: New York, 1989.

(19) Slater, J. C. *Physical Review* **1930**, *35*, 509.

(20) Slater, J. C. *Physical Review* **1929**, *34*, 1293.

(21) Bytautas, L.; Nagata, T.; Gordon, M. S.; Ruedenberg, K. *Journal of Chemical Physics* **2007**, *127*, 164317/1.

(22) Roothaan, C. C. J. *Reviews of Modern Physics* **1951**, *23*, 69.

(23) McWeeny, R.; Diercksen, G. *Journal of Chemical Physics* **1968**, *49*, 4852.

(24) Guest, M. F.; Saunders, V. R. *Molecular Physics* **1974**, *28*, 819.

(25) Binkley, J. S.; Pople, J. A.; Dobosh, P. A. *Molecular Physics* **1974**, *28*, 1423.

(26) Hsu, H.-L.; Davidson, E. R.; Pitzer, R. M. *Journal of Chemical Physics* **1976**, *65*, 609.

(27) Davidson, E. R. *Chemical Physics Letters* **1973**, *21*, 565.

(28) Faegri, K., Jr.; Manne, R. *Molecular Physics* **1976**, *31*, 1037.

(29) Pople, J. A.; Nesbet, R. K. *Journal of Chemical Physics* **1954**, *22*, 571.

(30) Ivanic, J.; Ruedenberg, K. *Theoretical Chemistry Accounts* **2001**, *106*, 339.

(31) Brooks, B. R.; Laidig, W. D.; Saxe, P.; Handy, N. C.; Schaefer, H. F., III. *Physica Scripta* **1980**, *21*, 312.

(32) Brooks, B. R.; Schaefer, H. F., III. *Journal of Chemical Physics* **1979**, *70*, 5092.

(33) Ivanic, J. *Journal of Chemical Physics* **2003**, *119*, 9364.

(34) Moller, C.; Plesset, M. S. *Physical Review* **1934**, *46*, 618.

(35) Lee, T. J.; Jayatilaka, D. *Chemical Physics Letters* **1993**, *201*, 1.

(36) Lee, T. J.; Rendell, A. P.; Dyall, K. G.; Jayatilaka, D. *Journal of Chemical Physics* **1994**, *100*, 7400.

(37) Coester, F.; Kummel, H. *Nuclear Physics* **1960**, *17*, 477.

(38) Cizek, J.; Paldus, J. *Physica Scripta* **1980**, *21*, 251.

(39) Purvis, G. D., III; Bartlett, R. J. *Journal of Chemical Physics* **1982**, *76*, 1910.

(40) Piecuch, P.; Kucharski, S. A.; Kowalski, K.; Musial, M. *Computer Physics Communications* **2002**, *149*, 71.

(41) Raghavachari, K.; Trucks, G. W.; Pople, J. A.; Head-Gordon, M. *Chemical Physics Letters* **1989**, *157*, 479.

(42) Wloch, M.; Gour, J. R.; Piecuch, P. *Journal of Physical Chemistry A* **2007**, *111*, 11359.

CHAPTER 2. EXPLORING THE EFFECT OF ANHARMONICITY OF MOLECULAR VIBRATIONS ON THERMODYNAMIC PROPERTIES

A paper published in *The journal of Chemical Physics*

Bosiljka Njegic and Mark S. Gordon

Abstract

Thermodynamic properties of selected small and medium size molecules were calculated using harmonic and anharmonic vibrational frequencies. Harmonic vibrational frequencies were obtained by normal mode analysis, whereas anharmonic ones were calculated using the vibrational self-consistent field, VSCF, method. The calculated and available experimental thermodynamic data for zero point energy (ZPE), enthalpy, entropy and heat capacity are compared. It is found that the anharmonicity and coupling of molecular vibrations can play a significant role in predicting accurate thermodynamic quantities. Limitations of the current VSCF method for low frequency modes have been partially removed by following normal mode displacements in internal, rather than Cartesian, coordinates.

I. Introduction

Ab initio calculations provide data that can be used in evaluating, interpreting or predicting experimental results pertaining to spectral and thermodynamic properties of molecules. This is especially important for larger molecules, for which obtaining and identifying all vibrational frequencies from experiment alone is quite

often a very difficult task. Calculated frequencies and their intensities may be used to simulate vibrational spectra and compare them to experimental data to assign the experimental frequencies. Furthermore, the calculated frequencies can also be used to calculate thermodynamic properties that are not easy to obtain experimentally, and which impact the accuracy of *ab initio* calculations such as enthalpies of formation, reaction enthalpies, and activation energies.

The goal of the present work is to explore the effect of anharmonicity and coupling of molecular vibrations on the accuracy of calculated thermodynamic properties. Anharmonic, coupled vibrational frequencies were calculated using the vibrational self-consistent field (VSCF) method, which was first introduced in late 1970's[1-4] and further developed into the *ab initio* VSCF method with a second order perturbation theory correction[5-9] that is used in the present work.

For some species, low vibrational frequencies calculated by the VSCF method overestimate experimental values by such a magnitude that it is impossible to obtain reliable thermodynamic properties. For these cases a different approach for generating the PES, in which normal modes are displaced in internal[10], rather than Cartesian[11] coordinates, is shown to be more reliable.

II. Computational Methods

A. Thermodynamic functions

Statistical thermodynamics is used to obtain macroscopic properties such as enthalpy, entropy, and heat capacity from molecular energy level *ab initio* calculations. Formulas for the thermodynamic functions of interest are summarized

in Table I. Molecular partition functions can be expressed as products of translational, rotational and vibrational partition functions, assuming that these types of motion are separable and noting that usually the electronic partition function can be taken as the degeneracy of the ground electronic state, which is unity for closed shell molecules. The rotational and translational partition functions were obtained using the usual rigid rotor – ideal gas approximations. Although vibrational thermodynamic functions apply rigorously only within the harmonic approximation, anharmonic frequencies can, as noted by Truhlar and Isaacson[12-14], be used to construct a simple approximation to the correct vibrational partition functions. This approximation has been shown to provide good agreement with more rigorous calculations[12-17]. Among all thermodynamic properties entropy is, as shown in the Appendix A, particularly sensitive to changes in low vibrational frequencies, which are frequently the most heavily affected by anharmonicity and coupling.

One can calculate the zero point vibrational energy (ZPE) in more than one way. A simple approach is to use the anharmonic frequencies in the simple (harmonic) energy expression given in Table I, where ν_i are the anharmonic frequencies obtained from VSCF calculations[5,9], as suggested by Truhlar and Isaacson[12-14]. Alternatively, one can employ the VSCF vibrational energy levels to calculate the ZPE. The first method is consistent with both the approach described above for calculating the thermodynamic properties and the manner in which ZPE are reported in the NIST data base[18], while the second method is directly related to the VSCF approach. Both sets of zero point energies are reported below.

B. Vibrational self-consistent field method, VSCF

The foundation for the VSCF method is obtaining an accurate potential energy surface. As there is no analytic expression for the PES, one needs to calculate it on a grid. In order to choose grid points, the first step is to calculate the equilibrium geometry to obtain a starting point from which the potential energy surface of the molecule may be explored. Then, a normal mode analysis at this structure provides normal mode frequencies and normal mode displacements, which define, respectively, how far and in which direction the PES will be explored. A normal mode displacement can be expressed in terms of Cartesian or internal coordinates (e.g., bond lengths, angles and torsions). Since normal modes are delocalized, with more than one internal coordinate involved in a particular vibrational motion, one can express each vibrational motion as a sum of contributions of all internal coordinates, such that this sum satisfies completeness and symmetry requirements.

As the normal mode analysis is done in the harmonic approximation without coupling of molecular vibrations, one may generate the PES by making two types of displacements from the equilibrium geometry: along each normal mode separately or along two or more normal modes simultaneously. The first type of displacement generates the so-called diagonal potential, which reflects the anharmonicity along each normal mode. The second type of displacement gives rise to the coupling potential, which measures the coupling of vibrations involved in the displacement.

There are several approaches for generating a PES on a grid. Two of these were employed in this work, namely direct and QFF methods. In the direct approach[5]

electronic structure calculations are done at 16 points along each normal mode to explore anharmonicity of the particular mode, and 16x16 grid points following the simultaneous displacements along two normal modes in order to describe pair-wise coupling of molecular vibrations. The direct method yields accurate results, but it is computationally very demanding, so for larger molecules the PES was generated in the quartic force field (QFF) approximation[9], a fourth order Taylor expansion of the PES as a function of mass-weighted normal coordinates. The expansion coefficients are determined by differentiation of the energy, which requires electronic structure calculations at only 6 points along each normal mode and 12 points along each pair of normal modes. These expansion coefficients are then used to calculate the potential for 16 points along each normal mode and 16x16 grid points for pair-wise coupling. The obtained PES is used to solve the vibrational Schrödinger equation in mass-weighted normal coordinates, Q_i given by:

$$\hat{\mathrm{H}}_{vib}\Psi_n(Q_1,...,Q_f) = \mathrm{E}_n\Psi_n(Q_1,...,Q_f), \tag{18}$$

where the vibrational Hamiltonian, $\hat{H}_{vib}$ is:

$$\hat{\mathrm{H}}_{vib} = -\frac{1}{2}\sum_{i=1}^{f}\frac{\partial^2}{\partial Q_i^{\,2}} + V(Q_1,...,Q_f). \tag{19}$$

The VSCF method is based on the separability of normal mode vibrations:

$$\Psi_n(Q_1,...,Q_f) = \prod_{i=1}^{f}\psi_i^{(n)}(Q_i). \tag{20}$$

One can then rewrite the Schrödinger equation in terms of a set of single-mode VSCF equations:

$$\left[-\frac{1}{2}\frac{\partial^2}{\partial Q_i^{\,2}}+\bar{V}_i^{(n)}(Q_i)\right]\psi_i^{(n)}(Q_i)=\varepsilon_i^{(n)}\psi_i^{(n)}(Q_i), \tag{21}$$

where $\bar{V}_i^{(n)}(Q_i)$ is an effective potential energy operator,

$$\bar{V}_i^{(n)}(Q_i)=\left\langle\prod_{j\neq i}^{f}\psi_j^{(n)}(Q_j)\middle|V(Q_1,...,Q_f)\middle|\prod_{j\neq i}^{f}\psi_j^{(n)}(Q_j)\right\rangle. \tag{22}$$

The potential energy, $V(Q_1,...,Q_f)$ is a sum of diagonal and coupling potentials calculated on the grid:

$$V(Q_1,...,Q_f)=\sum_{i=1}^{f}V_i(Q_i)+\sum_{i}\sum_{j<i}^{f}V_{ij}(Q_i,Q_j). \tag{23}$$

Eqs (21) and (22) are solved self-consistently using the collocation method[19] to obtain the vibrational energy levels at the VSCF level of theory:

$$E_n^{VSCF}=\sum_{i=1}^{f}\varepsilon_i^{(n)}-(f-1)\times\left\langle\prod_{i=1}^{f}\Psi_i^{(n)}(Q_i)\middle|V(Q_1,...,Q_f)\middle|\prod_{i=1}^{f}\Psi_i^{(n)}(Q_i)\right\rangle. \tag{24}$$

In this sense, the VSCF equations are analogous to the Hartree-Fock equations in electronic structure theory. From this analogy, it follows that the VSCF method alone will not generally provide sufficient accuracy. One approach for further improvement is to employ second order perturbation theory. The second order perturbation theory corrected vibrational energy levels, VSCF-PT2, are given by

$$E_n^{VSCF-PT2}=E_n^{VSCF}+\sum_{m\neq n}\frac{\left|\left\langle\prod_{i=1}^{f}\psi_i^{(n)}(Q_i)\middle|\Delta V\middle|\prod_{i=1}^{f}\psi_i^{(m)}(Q_i)\right\rangle\right|^2}{E_n^{(0)}-E_m^{(0)}}, \tag{25}$$

where the perturbation potential, ΔV, is:

$$\Delta V=V(Q_1,...,Q_f)-\sum_{i=1}^{f}\bar{V}_i^{(n)}(Q_i),$$

and the $E_n^{(0)}$ and $E_m^{(0)}$ are the sums of single mode energies in the reference and excited states, respectively.

Anharmonic, coupled VSCF-PT2 vibrational frequencies, are obtained as fundamental excitations from vibrational energy levels calculated at the VSCF-PT2 level of theory[5,9].

III. Computational details

All computations were done using the GAMESS program suite[20,21], and molecules were visualized in MacMolPlt[22].

The basis sets used in this work include 6-31G(d,p)[23,24], MIDI[25], pVTZ[26-29] with diffuse functions[30], aug-cc-pVDZ[31-35] and aug-cc-pVTZ[31-35], with the Hartree-Fock (RHF[36]), second order perturbation theory (MP2[37-41]) or coupled cluster (CCSD(T)[42]) levels of theory. Details are given in the tables in the following section. The calculations on homonuclear and heteronuclear diatomic molecules employed D_{4h} and C_{4v} symmetry, respectively, while the remaining molecules were considered in their full point groups. Additional details can be found in Fig. 1.

The geometries for all of the molecules studied were tightly optimized[43-45] with the largest component of the gradient required to be less than $1x10^{-5}$ Hartree/bohr. CCSD(T) geometry optimizations were accomplished using numerical gradients. A normal mode analysis[11] was performed, and the resulting harmonic frequencies and normal mode displacements were used to generate the PES on a 16x16 grid. VSCF calculations[5,9] were done yielding anharmonic, VSCF-PT2 frequencies. Harmonic

frequencies and VSCF-PT2 frequencies were then used to calculate thermodynamic properties of the molecules.

Two sets of calculations were performed to generate potential energy surfaces. For the first set of calculations harmonic frequencies and normal mode displacements in Cartesian coordinates were used to generate a PES on a grid directly[5] for all except the larger molecules such as $(H_2O)_6$, $((OH)_2HSi)_2O$, $(H_2SiO)_3$, and $(H_2SiO)_4$ where a QFF[9] generated PES was used instead. For the second set of calculations, for water, water dimer, sulfuric acid and urea, normal mode displacements in both internal and Cartesian coordinates were used to generate a direct PES[5]. For infinitesimal displacements, there is no difference between the use of Cartesian or internal coordinates. However, since the VSCF procedure involves several finite steps along each normal mode direction, different points on the potential energy surface (PES) are sampled, depending on whether Cartesian or internal coordinates are employed. The larger the displacement, the more important this distinction becomes. For stiff modes with high vibrational frequencies, small linear (Cartesian) displacements provide a reasonable accounting of the region of the PES sampled during the VSCF procedure. For low frequency modes, frequently dominated by angle bends and torsions, a more sensible region of the PES is sampled if one chooses internal coordinates. A more rigorous approach, as discussed in detail by Gerber and co-workers[46-49], would be to reformulate the vibrational Hamiltonian in terms of internal or angular coordinates. However, it is shown below that the simple procedure used here can be very effective.

IV. Results and Discussions

Molecules were chosen for this study based on the availability of experimental data, as well as the likelihood that some vibrational modes would exhibit significant anharmonicity. The latter include molecules with anharmonic modes due to hydrogen bonding, such as water dimer, $(H_2O)_2$ and hydrogen-fluoride dimer, $(HF)_2$, as well as some larger cyclic molecules with floppy vibrational motions, such as cyclotrisiloxane, $(H_2SiO)_3$ and cyclotetrasiloxane, $(H_2SiO)_4$ (See Fig. 1). The largest molecule studied was the cyclic water hexamer, $(H_2O)_6$ that combines both hydrogen bonding and floppy motions (Fig. 1f).

Zero point energies (ZPE), enthalpy (ΔH^0) and entropy (ΔS^0) are given in Tables II-IV, while heat capacity (C^0_p) data are tabulated in Table VIII. Subscripts har, anh and cal(expfreq) represent calculations that employ a particular basis set and level of theory in which harmonic, anharmonic or experimental frequencies, respectively, were used in partition functions in the rigid rotor-harmonic oscillator approximation. ZPE and thermodynamic properties calculated using experimental frequencies represent the limits of the approach in which harmonic partition functions are used. The subscript exp stands for experimental data.

A. Diatomic molecules

First, consider diatomic molecules. Heavier molecules, such as Cl_2, Br_2 and I_2, do not exhibit significant anharmonic effects on the ZPEs. As shown in Table II, the ZPEs are very similar, regardless of the computational method: harmonic (ZPE_{har}), anharmonic (ZPE_{anh}), experimental frequencies ($ZPE_{cal(expfreq)}$), VSCF

energy level calculations ($ZPE(0)_{ELC}$), or anharmonic ZPE calculated from an expansion in anharmonic constants[50] (ZPE_{exp}). On the other hand, light molecules such as H_2, HF and F_2 do show discrepancies between ZPE_{har} and ZPE_{anh}, with the latter being closer to ZPE calculated from experimental frequencies.

Different levels of theory and different basis sets were utilized in order to explore convergence of ZPE_{anh} to $ZPE_{cal(expfreq)}$ for these light diatomic molecules. The MP2 level of theory with the small 6-31G(d,p) basis set gives better agreement than MP2 with the larger aug-cc-pVTZ basis set. On the other hand, CCSD(T) with the larger basis set gives excellent agreement between ZPE_{anh} and $ZPE_{cal(expfreq)}$, while ZPE_{har} is off by ~0.25 kcal/mol, so that high accuracy in fundamental frequencies is achieved by including both very accurate electronic structure theory and a proper accounting for anharmonicity. The deterioration of MP2 predictions with improvements in the basis set has been noted previously[51]. It is likely that an even better basis set is needed to reach convergence of $ZPE(0)_{ELC}$ to ZPE_{exp} for very light molecules like H_2 and HF.

Although H_2, HF and F_2 do show significant anharmonicity, thermodynamic properties such as enthalpy, entropy and heat capacity are well described in the harmonic approximation for all diatomic molecules (see Tables III, IV, and VIII). Since the thermodynamic properties of interest are inversely proportional to the frequencies, changes in high frequencies due to anharmonicity do not result in significant changes in thermodynamic properties.

B. Molecules with stiff modes

Next, consider molecules with relatively stiff vibrational motions, such as H_2O, NH_3 and CH_4, or a relatively small degree of anharmonicity, as in H_2O_2, H_2S_2, H_2SO_4, CH_3NO_2 and urea (Table II). Comparison of ZPE_{har} and ZPE_{anh} with $ZPE_{cal(expfreq)}$ demonstrates that ZPE_{anh} is ~1 kcal/mol more accurate than ZPE_{har}, because the calculated anharmonic vibrational frequencies are more accurate than harmonic ones. Next, compare ZPE_{anh} and $ZPE(0)_{ELC}$, obtained from vibrational energy level calculations, with ZPE_{exp}, obtained by extrapolation from experimental vibrational levels. For H_2O and H_2O_2, $ZPE(0)_{ELC}$ is ~0.2 kcal/mol and ~0.6 kcal/mol, respectively, closer to ZPE_{exp} than ZPE_{anh}. Indeed, in general, the two methods used to calculate ZPE based on VSCF anharmonic frequencies are in very good agreement with each other at least for molecules with stiff vibrations, although if one strives for high accuracy the method of choice should be $ZPE(0)_{ELC}$.

Thermodynamic properties for polyatomic molecules with primarily stiff modes, such as water, ammonia and methane, (Tables III. IV, and VIII) not exhibit significant discrepancies among the values calculated using the harmonic formula with harmonic, VSCF-PT2, or experimental frequencies, vs. experimental data. The enthalpy (Table III) is well described in the harmonic approximation, with errors relative to experiment lower than 0.2 kcal/mol. This error can be reduced to < 0.1 kcal/mol by using the harmonic partition function formula with accurate anharmonic frequencies ($\Delta H_{cal(expfreq)}$).

Comparison of entropy values listed in Table IV for H_2S_2, CH_3NO_2 and urea shows the following trend in errors compared to experimental data: $S^0_{har} > S^0_{anh} >$

$S^0_{cal(expfreq)}$. This is to be expected, since the entropy is more sensitive to changes in low frequencies that are treated more accurately when anharmonicity is included in the calculation. Note that an unexpectedly high S^0_{anh} is obtained for H_2SO_4. This is due to the error encountered when one uses Cartesian displacements in the VSCF-PT2 calculations for low frequency modes. This will be discussed in more detail below.

Although the main focus of this paper is on comparisons of calculated thermodynamic properties with available experimental data, it is worth mentioning the theoretical results obtained by Truhlar *et al.* employing accurate vibrational-rotational partition functions for CH_4[52] and H_2O_2[53,54] molecules. The calculated vibrational partition functions obtained in this work for CH_4, 1.004 and 1.005 in the harmonic and anharmonic approximations, respectively. Both are in very good agreement with the 1.008 predicted by Truhlar *et al.* value. This is to be expected at room temperature, since, as noted by Truhlar et al., the rigid-rotor-harmonic-oscillator approximation is already very close to the accurate rotovibrational partition function due to the lack of floppy modes in CH_4. For H_2O_2, the calculated $ZPE(0)_{ELC}$=16.46 kcal/mol is in very good agreement with the value of ~16.37 kcal/mol estimated by Truhlar *et al.*[54]. Finally, the calculated room temperature standard-state Gibbs free energy of 13.64 kcal/mol underestimates by less than 0.5 kcal/mol the more accurate values obtained by Truhlar et al.[53] and Dorofeeva *et al.*[55].

C. Molecules with low frequency modes

Now, consider larger, highly anharmonic systems with hydrogen bonding and other floppy motions. These molecules are listed in Tables II-IV starting with $(HF)_2$ and ending with $(H_2SiO)_4$. ZPE_{har} and ZPE_{anh} differ by ~0.4-1.4 kcal/mol (Table II). Similar differences are observed among harmonic and anharmonic enthalpies, entropies and heat capacities (Tables III, IV, and VIII). Unfortunately, there is little available experimental data for comparison. Reported experimental entropies for $(HF)_2$ range from 57.08[50] to 62.36[18] cal/mol-K, and experimental heat capacities for this species range from 10.71[50]-13.89[18] cal/mol-K. The calculated values are in the upper ends of these ranges. Nevertheless, it is interesting to note that for all these molecules, thermodynamic properties calculated with anharmonic frequencies have lower values than those calculated using harmonic frequencies. In the absence of experimental data, this is surprising. Generally, one expects that anharmonicity and coupling will both lower vibrational frequencies and consequently increase the enthalpy, entropy and heat capacity. Since these three thermodynamic properties increase as frequencies decrease, the observed trend should be the reverse of the predictions for these species.

The origin of this unusual behavior lies in the manner in which low frequency motions are treated in the usual VSCF computation of the PES. Comparison of VSCF-PT2 frequencies with experimental frequencies shows that coupling and anharmonicity for $(H_2O)_2$ and $(HF)_2$ are overestimated by the VSCF method. This results in predicted frequencies that can be much too high, as illustrated in Table V. For example, for water dimer the three lowest VSCF-PT2 frequencies lying below

200 cm^{-1} calculated employing normal mode displacements in Cartesian coordinates (VSCF-PT2(cart)) give values that overestimate experimental frequencies by 200-300 cm^{-1}, while harmonic frequencies are off by less than 60 cm^{-1}. It is revealing that VSCF-PT2(cart) gives much better agreement with experimental bond-stretching frequencies than with angle bends or torsions, even though the bond stretches may also be low frequency. An example is the hydrogen bonded intermolecular stretch in $(H_2O)_2$ which is better described with VSCF-PT2(cart) with an error of 20 cm^{-1} vs. the harmonic approximation error of 40 cm^{-1}.

So, in general, low frequency bending and torsion motions are better described in the harmonic approximation than by VSCF-PT2 with a PES based on normal mode displacements in Cartesian coordinates. One approach to solving this problem[56] might be to use harmonic frequencies for low frequency modes that are dominated by angle bends and torsions, rather than VSCF-PT2 frequencies. However, this is not a general (or satisfying) solution, since low frequency modes can be rather mixed. Of course, the most desirable approach would be to reformulate the vibrational Hamiltonian in terms of curvilinear coordinates[46,48,57,58], but this is difficult to accomplish in the general case.

D. Cartesian versus internal displacement coordinates

To a large degree, the origin of the partial failure of the VSCF approach lies not in the VSCF method itself, but rather in the manner in which the potential energy surface is generated, since the quality of the results can only be as good as the calculated PES. The VSCF method consists of two crucial steps: (1) the calculation

of the diagonal frequencies and (2) the calculation of the VSCF frequencies. Each diagonal frequency is calculated from PES grid points along the corresponding normal mode, whereas the VSCF frequencies depend on the PES along n normal modes, where n is the number of normal modes that are coupled in the calculation. This means that the diagonal frequencies and the associated PES grid points should reflect the anharmonicity of the corresponding normal mode, while the VSCF frequencies and the corresponding PES grid points should reflect the coupling of molecular vibrations. Since grid points determined from normal mode displacements in Cartesian coordinates do not preserve any particular internal coordinate, the calculated diagonal frequency does not correspond to a stretch, bend or torsion but rather to some mixture of these internal coordinates. Especially for low frequency/high amplitude vibrations, linear (Cartesian) displacements will therefore not capture the correct potential energy surface. The linear displacements result in artificially high coupling of all vibrations since they all have mixed character. Because stretching motions are essentially linear, this problem primarily impacts bends and torsions. The latter are linear only for infinitesimal displacements, and the higher the amplitude of these types of vibrations, the worse the linear (Cartesian) displacements become.

Expanding the PES in terms of internal coordinate displacements can at least partially solve this problem. This new approach has been applied to water, water dimer, sulfuric acid and urea. Water dimer is of particular importance, because it has many floppy modes that cannot be successfully treated using Cartesian displacements.

Table V compares H_2O and $(H_2O)_2$ vibrational frequencies obtained by harmonic normal mode analysis (har), VSCF based on a PES generated in Cartesian (VSCF-PT2 cart) and internal (VSCF-PT2 int) displacements with experimental frequencies (exp). For water molecule, which has mostly stiff modes, there is still a small improvement when internal displacements are used, especially for the bend with the larger basis sets. Indeed, it seems to be a general trend that when one uses larger basis sets, the performance of internal vs. Cartesian displacements improves considerably. However, for H_2O, the bend frequency is ~ 1600 cm^{-1}, so an improvement of ~35 cm^{-1} (for internal vs. Cartesian displacements) has only a small effect on predicted thermodynamic properties (see Table VI). Calculated enthalpy and entropy are 2.37 kcal/mol and 45.09 cal/(mol•K), which are in excellent agreement with experimental data of [H(T)-H(0K)]=2.37 kcal/mol and S=45.13 cal/(K•T).

For $(H_2O)_2$, the use of smaller basis sets, such as 6-31G(d), with the use of internal displacements in the VSCF method introduces errors in the higher frequency modes, especially O-H stretches. As the basis set is improved to aug-cc-pVDZ, even the errors in these stiffer modes are smaller for internal displacements than for Cartesian displacements. For the weaker, intermolecular modes, for all basis sets, one observes very large errors when Cartesian displacements are employed, for the reasons discussed above. These errors range from ~200 to ~350 cm^{-1}. Following the normal mode displacements in internal coordinates lowers these errors to 50 cm^{-1} or less.

The impact of using internal vs. Cartesian displacements is illustrated in Fig. 2 for $(H_2O)_2$. Displacements relative to the equilibrium geometry, in terms of Cartesian or internal coordinates, for two modes of $(H_2O)_2$: the high frequency symmetric H-O stretch in the acceptor molecule (curves a, b) and the low frequency donor torsion vibration (curves c, d). Plotted on the y-axis are the energy changes due to each displacement. Plotted on the x-axis are the equally spaced displacements themselves, calculated as rms changes relative to the equilibrium geometry. The plotted displacements, in mass-weighted Cartesian coordinates, depend on whether the actual displacements are obtained in internals or Cartesians, since the internals are in general a composite of stretches, bends and torsions. There is a dramatic difference in the PES sampled along the low frequency donor torsion vibration, depending on whether Cartesian (curve c) or internal (curve d) displacements are employed. In contrast, the PES sampled along the high frequency H-O stretching mode is independent of which displacement coordinate is used, since curves a and b are essentially indistinguishable. Typically internal displacements (especially for angle bends and torsions) correspond to a tighter set of points (smaller displacements in Cartesian space) then do displacements that are obtained directly in Cartesian space.

More accurate frequencies are expected to lead to more accurate thermodynamic properties. There are no experimental data available for water dimer, however, experimental and calculated thermodynamic data for the reaction corresponding to water dimerization[59-64]are compared in Table VI. Since thermodynamic properties for water monomer are not significantly affected by a

small degree of anharmonicity, the calculated reaction enthalpy and entropy reflect the anharmonicity and coupling present in the water dimer. Although there is a need for more precise experimental measurements, the best calculated results (obtained from internal displacements along the PES) of ΔH=-3.27 kcal/mol and ΔS=-17.68 cal/(mol•K) are within the experimental error bars. These values were used to calculate $K_p=\exp(-\Delta H/RT+\Delta S/R)$. The calculated K_p=0.0113 atm^{-1} using internal displacements falls within the range of available experimental data[59-61]. Note that the use of Cartesian displacements produces thermodynamic properties for this reaction that are in much worse agreement with the experimental values. The values obtained using the harmonic approximation are not in as good agreement with experiment as are the VSCF-PT2 results if internal displacements are used, but (as noted above) the harmonic approximation is much better than VSCF-PT2 if one uses Cartesian displacements.

The calculated ΔH, ΔS and K_p reflect the important effect of anharmonicity and coupling of molecular vibrations on thermodynamic properties. Including the anharmonicity and vibration coupling lowers both enthalpy and (especially) entropy, as suggested in section IIA, thereby increasing K_p. This trend in entropy and K_p behavior is in accord with the published work of Muñoz-Caro and Niño[65], although their best calculated K_p=0.0034 atm^{-1} is too small compared to experiment, and they do report increase in ΔH with anharmonic correction.

Because sulfuric acid and urea are large molecules, only the modest 6-31G(d,p) basis set was used with MP2 for VSCF calculations on these molecules.

Table VII lists the experimental and calculated vibrational frequencies for H_2SO_4. As noted for water dimer, the predicted frequencies for the stiffer modes deteriorate a bit. Based on the water dimer calculations, this would be corrected if a larger basis set was used. On the other hand, the use of Cartesian displacements for the lower frequency modes leads to very poor frequencies, whereas there is considerable improvement when internal displacements are used. This suggests that better basis sets are required to obtain consistently reliable VSCF calculations with internal displacements. The analogous comparison for urea is similar, although the error for the smallest known experimental frequency is larger for internal displacements than for Cartesian displacements. This may have several origins, including the need for better atomic basis sets, for higher order coupling of vibrational modes, the use of curvilinear coordinates for mapping out the potential energy surface, and possible inaccuracies in the experimental frequencies.

V. Conclusions

This paper has explored the influence of anharmonicity of molecular vibrations, as calculated by the VSCF-PT2 method, on thermodynamic properties. Entropy and heat capacity appear to be the most greatly affected by anharmonicity, although an anharmonic treatment of molecular vibrations is also important for quantitative *ab initio* calculations of other thermodynamic quantities. All calculations described here have been implemented in GAMESS[20,21].

In general, the use of internal displacements to generate the VSCF potential energy surface is more reliable than the use of Cartesian coordinates. For higher frequency modes, the accuracy of frequencies obtained with internal coordinate displacements improves dramatically when the atomic basis set and the level of theory are improved. Based on the calculations presented here, internal displacements are preferred to Cartesian displacements for mapping out the potential energy surface when low frequency floppy modes are present in the molecular system of interest.

Acknowledgements

This work was supported by a grant from the Air Force Office of Scientific Research. The authors have benefited from several illuminating discussions with Professor Benny Gerber and Dr. Galina Chaban.

References

(1) Bowman, J. M. *Journal of Chemical Physics* **1978**, *68*, 608.

(2) Carney, G. D. *Advances in Chemical Physics* **1978**, *37*, 305.

(3) Cohen, M.; Greita, S.; McEachran, R. P. *Chemical Physics Letters* **1979**, *60*, 445.

(4) Gerber, R. B.; Ratner, M. A. *Chemical Physics Letters* **1979**, *68*, 195.

(5) Chaban, G. M.; Jung, J. O.; Gerber, R. B. *Journal of Chemical Physics* **1999**, *111*, 1823.

(6) Jung, J. O.; Gerber, R. B. *Journal of Chemical Physics* **1996**, *105*, 10332.

(7) Norris, L. S.; Ratner, M. A.; Roitberg, A. E.; Gerber, R. B. *Journal of Chemical Physics* **1996**, *105*, 11261.

(8) Matsunaga, N.; Chaban, G. M.; Gerber, R. B. *Journal of Chemical Physics* **2002**, *117*, 3541.

(9) Yagi, K.; Hirao, K.; Taketsugu, T.; Schmidt, M. W.; Gordon, M. S. *The Journal of Chemical Physics* **2004**, *121*, 1383.

(10) Boatz, J. A.; Gordon, M. S. *Journal of Physical Chemistry* **1989**, *93*, 1819.

(11) Gwinn, W. D. *Journal of Chemical Physics* **1971**, *55*, 477.

(12) Kuhler, K. M.; Truhlar, D. G.; Isaacson, A. D. *Journal of Chemical Physics* **1996**, *104*, 4664.

(13) Isaacson, A. D.; Truhlar, D. G. *Journal of Chemical Physics* **1981**, *75*, 4090.

(14) Truhlar, D. G.; Isaacson, A. D. *Journal of Chemical Physics* **1991**, *94*, 357.

(15) Isaacson, A. D.; Zhang, X. *Theoretica Chimica Acta* **1988**, *74*, 493.

(16) Isaacson, A. D.; Hung, S.-C. *Journal of Chemical Physics* **1994**, *101*, 3928.

(17) Isaacson, A. D. *Journal of Chemical Physics* **1998**, *108*, 9978.

(18) Russell, D. J. I. *NIST Computational Chemistry Comparison and Benchmark Database, NIST Standard Reference Database Number 101*, 2005.

(19) Yang, W.; Peet, A. C. *Journal of Chemical Physics* **1990**, *92*, 522.

(20) Dykstra, C. E.; Frenking, G.; Kim, K. S.; Scuseria, G. E.; Editors *Theory and Applications of Computational Chemistry: The First Forty Years*, 2005.

(21) Schmidt, M. W.; Baldridge, K. K.; Boatz, J. A.; Elbert, S. T.; Gordon, M. S.; Jensen, J. H.; Koseki, S.; Matsunaga, N.; Nguyen, K. A.; et al. *Journal of Computational Chemistry* **1993**, *14*, 1347.

(22) Bode, B. M.; Gordon, M. S. *Journal of Molecular Graphics & Modelling* **1998**, *16*, 133.

(23) Hariharan, P. C.; Pople, J. A. *Theoretica Chimica Acta* **1973**, *28*, 213.

(24) Francl, M. M.; Pietro, W. J.; Hehre, W. J.; Binkley, J. S.; Gordon, M. S.; DeFrees, D. J.; Pople, J. A. *Journal of Chemical Physics* **1982**, *77*, 3654.

(25) Huzinaga, S.; Andzelm, J. *Gaussian basis sets for molecular calculations*; Elsevier: Amsterdam ; New York, 1984.

(26) Dunning, T. H., Jr. *Journal of Chemical Physics* **1971**, *55*, 716.

(27) McLean, A. D.; Chandler, G. S. *Journal of Chemical Physics* **1980**, *72*, 5639.

(28) Wachters, A. J. H. *Journal of Chemical Physics* **1970**, *52*, 1033.

(29) Rappe, A. K.; Smedley, T. A.; Goddard, W. A., III. *Journal of Physical Chemistry* **1981**, *85*, 2607.

(30) Clark, T.; Chandrasekhar, J.; Spitznagel, G. W.; Schleyer, P. v. R. *Journal of Computational Chemistry* **1983**, *4*, 294.

(31) Dunning, T. H., Jr. *Journal of Chemical Physics* **1989**, *90*, 1007.

(32) Woon, D. E.; Dunning, T. H., Jr. *Journal of Chemical Physics* **1994**, *100*, 2975.

(33) Woon, D. E.; Dunning, T. H., Jr. *Journal of Chemical Physics* **1993**, *98*, 1358.

(34) Koput, J.; Peterson, K. A. *Journal of Physical Chemistry A* **2002**, *106*, 9595.

(35) Kendall, R. A.; Dunning, T. H., Jr.; Harrison, R. J. *Journal of Chemical Physics* **1992**, *96*, 6796.

(36) Roothaan, C. C. J. *Reviews of Modern Physics* **1951**, *23*, 69.

(37) Pople, J. A.; Binkley, J. S.; Seeger, R. *International Journal of Quantum Chemistry, Symposium* **1976**, *10*, 1.

(38) Frisch, M. J.; Head-Gordon, M.; Pople, J. A. *Chemical Physics Letters* **1990**, *166*, 275.

(39) Fletcher, G. D.; Schmidt, M. W.; Gordon, M. S. *Advances in Chemical Physics* **1999**, *110*, 267.

(40) Aikens, C. M.; Gordon, M. S. *Journal of Physical Chemistry A* **2004**, *108*, 3103.

(41) Aikens, C. M.; Webb, S. P.; Bell, R. L.; Fletcher, G. D.; Schmidt, M. W.; Gordon, M. S. *Theoretical Chemistry Accounts* **2003**, *110*, 233.

(42) Piecuch, P.; Kucharski, S. A.; Kowalski, K.; Musial, M. *Computer Physics Communications* **2002**, *149*, 71.

(43) Baker, J. *Journal of Computational Chemistry* **1986**, *7*, 385.

(44) Helgaker, T. *Chemical Physics Letters* **1991**, *182*, 503.

(45) Culot, P.; Dive, G.; Nguyen, V. H.; Ghuysen, J. M. *Theoretica Chimica Acta* **1992**, *82*, 189.

(46) Horn, T. R.; Gerber, R. B.; Ratner, M. A. *Journal of Chemical Physics* **1989**, *91*, 1813.

(47) Horn, T. R.; Gerber, R. B.; Ratner, M. A. *Journal of Physical Chemistry* **1993**, *97*, 3151.

(48) Horn, T. R.; Gerber, R. B.; Valentini, J. J.; Ratner, M. A. *Journal of Chemical Physics* **1991**, *94*, 6728.

(49) Bacic, Z.; Gerber, R. B.; Ratner, M. A. *Journal of Physical Chemistry* **1986**, *90*, 3606.

(50) Linstrom, P. J.; Mallard, W. G. *NIST Chemistry WebBook, NIST Standard Reference Database number 69*, 2005.

(51) Varganov, S. A.; Olson, R. M.; Gordon, M. S.; Metiu, H. *Journal of Chemical Physics* **2003**, *119*, 2531.

(52) Chakraborty, A.; Truhlar, D. G.; Bowman, J. M.; Carter, S. *Journal of Chemical Physics* **2004**, *121*, 2071.

(53) Lynch, V. A.; Mielke, S. L.; Truhlar, D. G. *Journal of Chemical Physics* **2004**, *121*, 5148.

(54) Lynch Vanessa, A.; Mielke Steven, L.; Truhlar Donald, G. *The journal of physical chemistry. A, Molecules, spectroscopy, kinetics, environment & general theory* **2005**, *109*, 10092.

(55) Dorofeeva, O. V.; Iorish, V. S.; Novikov, V. P.; Neumann, D. B. *Journal of Physical and Chemical Reference Data* **2003**, *32*, 879.

(56) Miller, Y.; Chaban, G. M.; Gerber, R. B. *Chemical Physics* **2005**, *313*, 213.

(57) Gibson, L. L.; Roth, R. M.; Ratner, M. A.; Gerber, R. B. *Journal of Chemical Physics* **1986**, *85*, 3425.

(58) Roth, R. M.; Gerber, R. B.; Ratner, M. A. *Journal of Physical Chemistry* **1983**, *87*, 2376.

(59) Curtiss, L. A.; Frurip, D. J.; Blander, M. *Journal of Chemical Physics* **1979**, *71*, 2703.

(60) Harvey, A. H.; Lemmon, E. W. *Journal of Physical and Chemical Reference Data* **2004**, *33*, 369.

(61) Evans, G. T.; Vaida, V. *Journal of Chemical Physics* **2000**, *113*, 6652.

(62) Scribano, Y.; Goldman, N.; Saykally, R. J.; Leforestier, C. *Journal of Physical Chemistry A* **2006**, *110*, 5411.

(63) Klopper, W.; van Duijneveldt-van de Rijdt, J. G. C. M.; van Duijneveldt, F. B. *Physical Chemistry Chemical Physics* **2000**, *2*, 2227.

(64) Tschumper, G. S.; Leininger, M. L.; Hoffman, B. C.; Valeev, E. F.; Schaefer, H. F., III; Quack, M. *Journal of Chemical Physics* **2002**, *116*, 690.

(65) Munoz-Caro, C.; Nino, A. *Journal of Physical Chemistry A* **1997**, *101*, 4128.

(66) Goubet, M.; Asselin, P.; Soulard, P.; Perchard, J. P. *Physical Chemistry Chemical Physics* **2003**, *5*, 5365.

(67) Day, M. B.; Kirschner, K. N.; Shields, G. C. *Journal of Physical Chemistry A* **2005**, *109*, 6773.

(68) Herzberg, G. *Molecular spectra and molecular structure*, 2d ed.; Van Nostrand: New York, 1950.

(69) Polyansky, O. L.; Csaszar, A. G.; Shirin, S. V.; Zobov, N. F.; Barletta, P.; Tennyson, J.; Schwenke, D. W.; Knowles, P. J. *Science (Washington, DC, United States)* **2003**, *299*, 539.

(70) Koput, J.; Carter, S.; Handy, N. C. *Journal of Physical Chemistry A* **1998**, *102*, 6325.

(71) Wagman, D. D.; Rossini, F. D. *Selected values of chemical thermodynamic properties*; [U.S. Dept. of Commerce, National Bureau of Standards]; for sale by the Superintendent of Documents, U.S. Govt. Print. Off.: Washington, 1965.

Fig. 1. MP2 optimized structures. Basis set is 6-31G(d,p), except for $(HF)_2$ where pVTZ with diffuse functions was used. a.) disiloxane, $(H_3Si)_2O$ in C_{2v}; b.) 1,1,3,3-disiloxanetetrol, $Si_2O_5H_6$ in C_1; cyclotrisiloxane, $(H_2SiO)_3$ in D_{3h}; d.) cyclotetrasiloxane, $(H_2SiO)_4$ in C_1; e.) water dimer, $(H_2O)_2$ in C_s; f.) water hexamer, $(H_2O)_6$ in C_1; g.) hydrogen fluoride dimer, $(HF)_2$ in C_s; h.) nitro-methane, CH_3NO_2 in C_1; i.) sulfuric acid, H_2SO_4 in C_2; k.) urea, $(H_2N)_2CO$ in C_2.

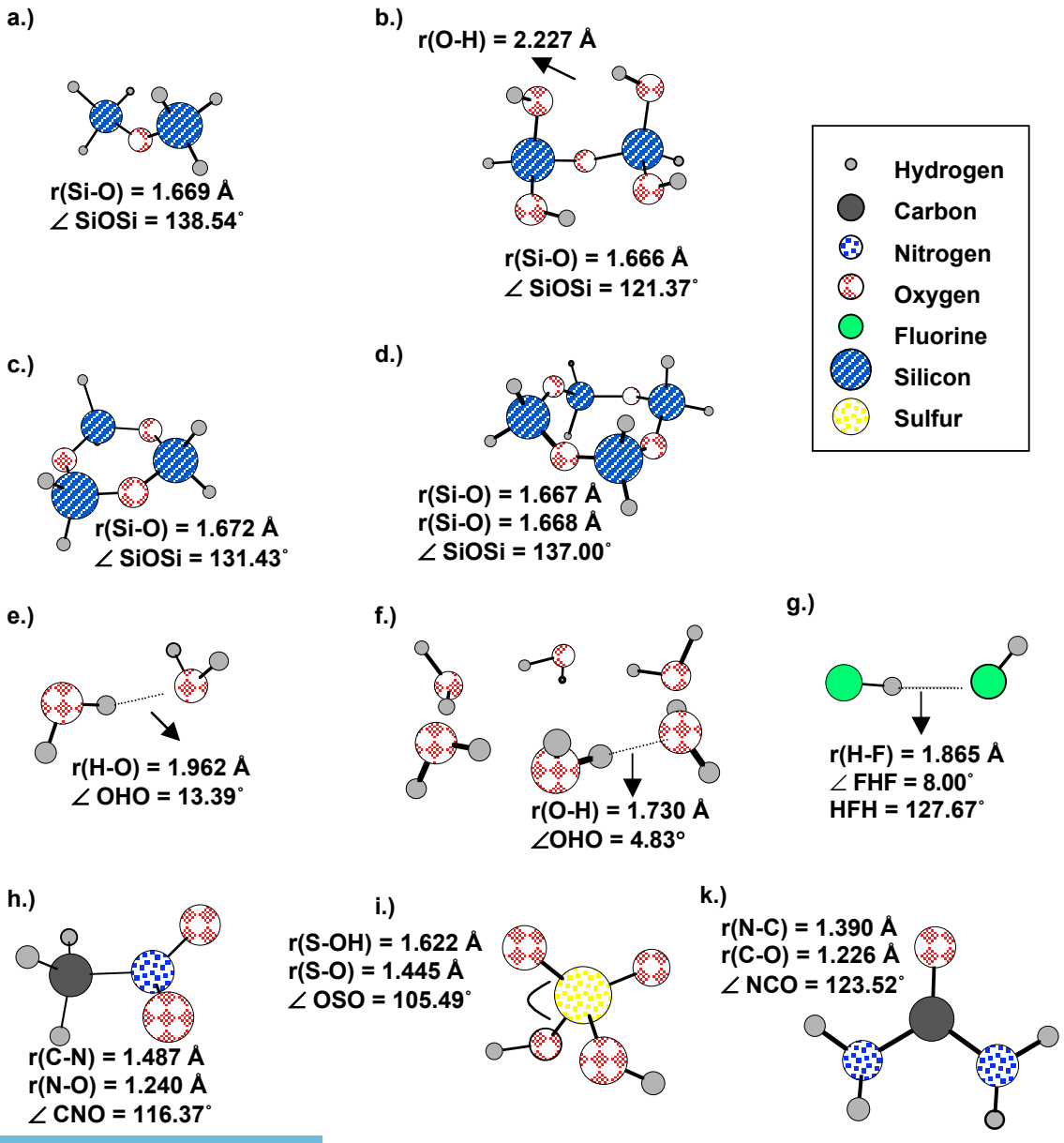

Figure 2. Potential energy surface sampled along stiff [(a) and (b)] symmetric H-O stretch in the acceptor molecule and along floppy [(c) and (d)] donor torsion vibrational modes. (a) Diagonal potential sampled along symmetric H-O stretch in the acceptor molecule by following normal mode displacements in Cartesian coordinates. (b) Diagonal potential sampled along symmetric H-O stretch by following normal mode displacement vectors in internal coordinates; (c) Diagonal potential sampled along donor torsion vibration by following normal mode displacements vectors in Cartesian coordinates; (d) Diagonal potential sampled along donor torsion vibration by following normal mode displacements in internal coordinates.

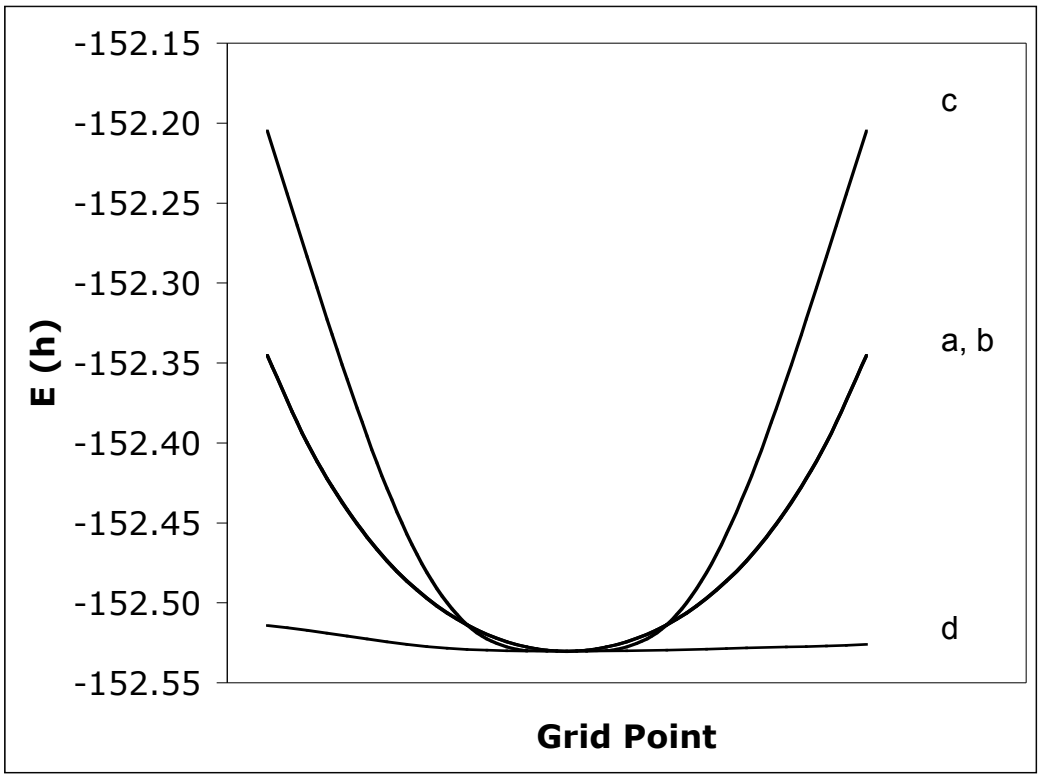

Table I. Thermodynamic functions. The volume V=RT/p, at pressure p and temperature T; R is the gas constant; m is the mass of the molecule; k is Boltzmann's constant; h is Planck's constant; I_A,I_B and I_C are the principle moments of inertia; σ is the symmetry factor; f is the number of vibrational degrees of freedom (3N-5 for linear and 3N-6 for non-linear molecule with N being the number of atoms in the molecule); ν_i is the i^{th} vibrational frequency.

Thermodynamic property	Function
Molecular partition function	$Q = Q_{tr}Q_{rot}Q_{vib}Q_{el}$
Translational partition function	$Q_{tr} = (2\pi mkT)^{3/2} h^{-3}V$
Translational enthalpy	$\left[H(T) - H(0)\right]_{tr} = (5/2)RT$
Translational entropy	$S_{tr} = R\left[(3/2)\ln\left(2\pi m/h^2\right) + (5/2)\ln(kT) - \ln(p) + 5/2\right]$
Translational heat capacity	$C_{p,tr} = (5/2)R$
Rotational partition function	$Q_{rot} = \frac{8\pi^2}{\sigma h^3}(2\pi kT)^{3/2}(I_A I_B I_C)$
Rotational enthalpy	$\left[H(T) - H(0)\right]_{rot} = (3/2)RT$
Rotational entropy	$S_{rot} = R\left[\ln\left(8\pi^2/\sigma\right) + (3/2)\ln\left(2\pi kT/h^2\right) + (1/2)\ln\left(I_A I_B I_C\right) + 3/2\right]$
Rotational heat capacity	$C_{p,rot} = (3/2)R$
Vibrational partition function	$Q_{vib} = \prod_{i=1}^{f}\left(1 - e^{-h\nu_i/kT}\right)^{-1}$
Vibrational enthalpy	$\left[H(T) - H(0)\right]_{vib} = RT\sum_{i=1}^{f}\left(\frac{h\nu_i}{kT}\right)\frac{e^{-h\nu_i/kT}}{\left(1 - e^{-h\nu_i/kT}\right)}$
Vibrational entropy	$S_{vib} = -R\sum_{i=1}^{f}\ln\left(1 - e^{-h\nu_i/kT}\right) + R\sum_{i=1}^{f}\left(\frac{h\nu_i}{kT}\right)\frac{e^{-h\nu_i/kT}}{\left(1 - e^{-h\nu_i/kT}\right)}$
Vibrational heat capacity	$C_{p,vib} = R\sum_{i=1}^{f}\left(\frac{h\nu_i}{kT}\right)^2\frac{e^{-h\nu_i/kT}}{\left(1 - e^{-h\nu_i/kT}\right)}$
Total enthalpy	$\left[H(T) - H(0)\right]_{tot} = \left[H(T) - H(0)\right]_{tr} + \left[H(T) - H(0)\right]_{rot} + \left[H(T) - H(0)\right]_{vib}$
Total entropy	$S_{tot} = S_{tr} + S_{rot} + S_{vib}$
Total heat capacity	$C_{p,tot} = C_{p,tr} + C_{p,rot} + C_{p,vib}$
Zero point energy	$ZPE = \frac{1}{2}\sum_{i=1}^{f}\nu_i$

Table II. Zero point energies (kcal/mol) [(δ(har-anh)=ZPE_{har}-ZPE_{anh}; δ(har-cal)=ZPE_{har}-$ZPE_{cal(expfreq)}$; δ (anh-cal)=ZPE_{anh}-$ZPE_{cal(expfreq)}$; δ (exp-cal)=ZPE_{exp}-$ZPE_{cal(expfreq)}$; δ(ELC-exp)=$ZPE(0)_{ELC}$-ZPE_{exp}] calculated using harmonic formula: harmonic (ZPE_{har}), anharmonic (ZPE_{anh}), experimental frequencies ($ZPE_{cal(expfreq)}$). Experimental frequencies are taken from Ref. [18] for all except diatomic molecules (Ref. [50]), $(HF)_2$ (Ref. [66]), H_2O_2 (Ref. [67]). $ZPE(0)_{ELC}$ is obtained directly from vibrational energy level calculations, whereas ZPE_{exp} is obtained from calculations using experimental constants for diatomic molecules (Ref. [68]) or in the case of water molecule from PES defined in Ref. [69], while H_2O_2 data is obtained from the variational results exchanged privately between Truhlar and Koput as published in Ref. [70].

Molecule	ZPE_{har}	ZPE_{anh}	$ZPE(0)_{ELC}$	$ZPE_{cal(expfreq)}$	ZPE_{exp}	δ(har-anh)	δ(har-cal)	δ(anh-cal)	δ(exp-cal)	δ(ELC-exp)
H_2[a]	6.59	6.26	6.53	5.94	6.38	0.33	0.64	0.32	0.43	0.15
H_2[c]	6.29	5.94	6.23	5.94	6.38	0.35	0.35	-0.01	0.43	-0.15
HF[a]	5.99	5.73	5.94	5.66	5.98	0.26	0.33	0.07	0.32	-0.04
HF[c]	5.90	5.65	5.84	5.66	5.98	0.25	0.24	-0.01	0.32	-0.14
F_2[a]	1.42	1.40	1.42	1.28	1.32	0.02	0.15	0.12	0.04	0.10
F_2[b]	1.43	1.41	1.43	1.28	1.32	0.03	0.16	0.13	0.04	0.11
F_2[c]	1.31	1.28	1.30	1.28	1.32	0.03	0.03	0.00	0.04	-0.02
Cl_2[a]	0.77	0.77	0.77	0.79	0.80	0.01	-0.02	-0.03	0.01	-0.03
Br_2[a]	0.47	0.47	0.47	0.47	0.47	0.00	0.01	0.00	0.00	0.00
I_2[d]	0.33	0.33	0.33	0.31	0.31	0.00	0.02	0.02	0.00	0.02
H_2O[a]	13.73	13.06	13.54	12.88	13.26	0.67	0.86	0.18	0.38	0.28
NH_3[a]	22.26	21.02	21.87	20.63		1.23	1.63	0.39		
CH_4[a]	29.20	28.22	28.83	27.11		0.99	2.10	1.11		
H_2O_2[a]	16.73	15.71	16.46	15.90	16.37	1.02	0.83	-0.20	0.47	0.09
H_2S_2[a]	12.14	11.61	11.97	11.16		0.53	0.98	0.45		
H_2SO_4[a]	24.70	23.37	24.70	23.91		1.33	0.79	-0.54		
CH_3NO_2[a]	32.32	31.55	32.13			0.77				
urea[a]	41.12	39.92	40.95	38.65		1.21	2.47	1.27		
$(HF)_2$[e]	13.69	14.11	14.25	12.81		-0.42	0.88	1.30		
$(H_2O)_2$[a]	29.73	29.34	30.44	27.51		0.38	2.22	1.84		
$(H_2O)_6$[a]	96.05	97.43	97.66			-1.38				
$(H_3Si)_2O$[a]	35.77	35.18	35.71			0.60				
$((HO)_2HSi)_2O$[a]	52.82	52.00	53.22			0.82				
$(H_2SiO)_3$[a]	44.18	43.77	44.08			0.41				
$(H_2SiO)_4$[a]	59.34	58.43	59.18			0.92				

Level of theory/basis set: [a]MP2/6-31G(d,p); [b]CCSD(T)/aug-cc-pVTZ; [c]MP2/aug-cc-pVTZ; [d]MP2/MIDI; [e]MP2/p-TZV with diffuse functions.

Table III. Enthalpy (kcal/mol) [(ΔH=[H(0K)-H(298.15K)]; δ(anh-cal)=ΔH^0_{anh}-$\Delta H^0_{cal(expfreq)}$; δ(har-anh)=ΔH^0_{har}-ΔH^0_{anh}; δ(har-exp)=ΔH^0_{har}-ΔH^0_{exp}; δ(anh-exp)=ΔH^0_{anh}-ΔH^0_{exp}; δ(cal-exp)=$\Delta H^0_{cal(expfreq)}$-$\Delta H^0_{exp}$] calculated using harmonic formula, with harmonic (ΔH^0_{har}), anharmonic, (ΔH^0_{anh}), and experimental frequencies ($\Delta H^0_{cal(freqexp)}$). Experimental frequencies are taken from Ref. [18] for all except diatomic molecules (Ref. [50]), $(HF)_2$ (Ref. [66]), and $(H_2O)_2$ (Ref. [67]). Experimental enthalpy is given as ΔH^0_{exp}. Experimental enthalpies are taken from Ref. [18], except for I_2 which is taken from Ref. [71].

Molecule	ΔH^0_{har}	ΔH^0_{anh}	$\Delta H^0_{cal(expfreq)}$	ΔH^0_{exp} [5]	δ(anh-cal)	δ(har-anh)	δ(har-exp)	δ(anh-exp)	δ(cal-exp)
H_2 [a]	2.07	2.07	2.07	2.02	0.00	0.00	0.05	0.05	0.05
H_2 [c]	2.07	2.07	2.07	2.02	0.00	0.00	0.05	0.05	0.05
HF [a]	2.07	2.07	2.07	2.06	0.00	0.00	0.01	0.01	0.01
HF [c]	2.07	2.07	2.07	2.06	0.00	0.00	0.01	0.01	0.01
F_2 [a]	2.10	2.10	2.11	2.11	-0.01	0.00	-0.01	-0.01	0.00
F_2 [b]	2.10	2.10	2.11	2.11	-0.01	0.00	-0.01	-0.01	0.00
F_2 [c]	2.11	2.11	2.11	2.11	0.00	0.00	0.00	0.00	0.00
Cl_2 [a]	2.20	2.20	2.19	2.19	0.01	0.00	0.01	0.00	0.00
Br_2 [a]	2.31	2.31	2.32	2.32	-0.01	0.00	-0.01	-0.01	-0.01
I_2 [d]	2.40	2.40	2.41	2.42	-0.01	0.00	-0.02	-0.02	-0.01
H_2O [a]	2.37	2.37	2.37	2.37	0.00	0.00	0.00	0.00	0.00
NH_3 [a]	2.39	2.40	2.40	2.40	-0.01	-0.01	-0.01	0.00	0.00
CH_4 [a]	2.39	2.39	2.40	2.39	-0.01	0.00	0.00	0.00	0.01
H_2O_2 [a]	2.65	2.67	2.63	2.67	0.04	-0.02	-0.02	0.00	-0.04
H_2S_2 [a]	2.72	2.75	2.76		-0.01	-0.03			
H_2SO_4 [a]	3.87	4.07	3.85	3.95	0.22	-0.20	-0.08	0.12	-0.10
CH_3NO_2 [a]	3.31	3.10		3.08		0.21	0.23	0.02	
urea [a]	3.28	3.30	3.46	3.49	-0.16	-0.01	-0.21	-0.19	-0.03
$(HF)_2$ [e]	3.41	3.04	3.54		-0.50	0.37			
$(H_2O)_2$ [a]	4.25	3.56	4.55		-0.99	0.69			
$(H_2O)_6$ [a]	10.23	8.22				2.01			
$(H_3Si)_2O$ [a]	4.35	4.13				0.21			
$((HO)_2HSi)_2O$ [a]	6.54	6.20				0.34			
$(H_2SiO)_3$ [a]	5.48	5.25				0.24			
$(H_2SiO)_4$ [a]	7.41	7.12				0.29			

Level of theory/basis set: [a]MP2/6-31G(d,p); [b]CCSD(T)/aug-cc-pVTZ; [c]MP2/aug-cc-pVTZ; [d]MP2/MIDI; [e]MP2/p-TZV with diffuse functions.

Table IV. Entropy (cal/mol*K) [δ(anh-cal)=S^0_{anh}-$S^0_{cal(expfreq)}$; δ(har-anh)=S^0_{har}-S^0_{anh}; δ(har-exp)=S^0_{har}-S^0_{exp}; δ (anh-exp)=S^0_{anh}-S^0_{exp}; δ (cal-exp)=$S^0_{cal(expfreq)}$-S^0_{exp}] calculated using harmonic formula with: harmonic (S^0_{har}), anharmonic (S^0_{anh}) and experimental frequencies ($S^0_{cal(expfreq)}$). Experimental frequencies are taken from Ref. [18], except diatomic molecules (Ref. [50]), $(HF)_2$ (Ref. [66]), and $(H_2O)_2$ (Ref. [67]). Experimental entropy is S^0_{exp}. Experimental entropies are taken from Ref. [18]; except for H_2O_2 (Ref. [50]) and I_2 (Ref. [71]).

Molecule	S^0_{har}	S^0_{anh}	$S^0_{cal(expfreq)}$	S^0_{exp} [4]	δ(anh-cal)	δ(har-anh)	δ(har-exp)	δ(anh-exp)	δ(cal-exp)
H_2[a]	31.08	31.08	31.08	31.23	0.00	0.00	-0.15	-0.15	-0.15
H_2[c]	31.13	31.13	31.13	31.23	0.00	0.00	-0.10	-0.10	-0.10
HF[a]	41.48	41.48	41.48	41.53	0.00	0.00	-0.05	-0.05	-0.05
HF[c]	41.48	41.48	41.48	41.53	0.00	0.00	-0.05	-0.05	-0.05
F_2[a]	48.40	48.41	48.45	48.47	-0.04	-0.01	-0.07	-0.06	-0.02
F_2[b]	48.34	48.34	48.44	48.47	-0.09	-0.01	-0.13	-0.13	-0.03
F_2[c]	48.42	48.44	48.39	48.47	0.05	-0.01	-0.05	-0.03	-0.08
Cl_2[a]	53.29	53.30	53.26	53.32	0.04	-0.01	-0.03	-0.02	-0.06
Br_2[a]	58.57	58.58	58.59	58.67	-0.01	-0.01	-0.10	-0.09	-0.08
I_2[d]	62.18	62.18	62.29	62.31	-0.11	-0.01	-0.13	-0.13	-0.02
H_2O[a]	45.09	45.09	45.06	45.13	0.03	0.00	-0.04	-0.04	-0.07
NH_3[a]	45.94	45.98	46.00	46.07	-0.02	-0.04	-0.13	-0.09	-0.07
CH_4[a]	44.43	44.44	44.46	44.54	-0.02	-0.01	-0.11	-0.10	-0.08
H_2O_2[a]	54.57	54.71	54.46	55.68	0.25	-0.14	-1.11	-0.97	-1.22
H_2S_2[a]	60.05	60.21	60.27	60.33	-0.06	-0.16	-0.28	-0.12	-0.06
H_2SO_4[a]	71.31	74.15	71.31	71.53	2.84	-2.85	-0.22	2.62	-0.22
CH_3NO_2[a]	69.38	65.61		65.77		3.77	3.61	-0.16	
urea[a]	64.82	65.01	65.92	66.42	-0.91	-0.19	-1.60	-1.41	-0.50
$(HF)_2$[e]	62.74	60.58	63.87	62.36	-3.29	2.16	0.38	-1.78	1.51
$(H_2O)_2$[a]	70.10	64.28	72.95		-8.67	5.82			
$(H_2O)_6$[a]	126.17	106.12				20.05			
$(H_3Si)_2O$[a]	77.23	73.11				4.12			
$((HO)_2HSi)_2O$[a]	94.21	91.32				2.90			
$(H_2SiO)_3$[a]	87.70	82.76				4.94			
$(H_2SiO)_4$[a]	107.47	101.83				5.64			

Level of theory/basis set: [a]MP2/6-31G(d,p); [b]CCSD(T)/aug-cc-pVTZ; [c]MP2/aug-cc-pVTZ; [d]MP2/MIDI; [e]MP2/p-TZV with diffuse functions.

Table V. MP2 vibrations of H_2O and $(H_2O)_2$. Experimental frequencies are taken from Ref. [18] for H_2O and Ref. [67] for $(H_2O)_2$. [acc: hydrogen acceptor molecule; donor: hydrogen donor molecule; ν1 refers to symmetric stretch, ν2 to bend, ν3 to asymmetric stretch; OPB: out-of-plane bend; IPB: in-plane bend; S: intermolecular stretch; AT: acceptor twist; AW: acceptor wag; DT: donor torsion.]

Water Monomer							
6-31G(d,p)	har	VSCF-PT2(cart)	VSCF-PT2(int)	exp	%err(har)	%err(anh) cart	%err(anh) int
asym str ν3	4033	3938	3948	3756	7.4	4.8	5.1
sym str ν1	3893	3803	3822	3657	6.5	4.0	4.5
bend ν2	1680	1622	1628	1595	5.3	1.7	2.1
aug-cc-pVDZ	har	VSCF-PT2(cart)	VSCF-PT2(int)	exp	%err(har)	%err(anh) cart	%err(anh) int
asym str ν3	3811	3717	3739	3756	1.5	1.0	0.5
sym str ν1	3711	3621	3651	3657	1.5	1.0	0.2
bend ν2	1615	1557	1562	1595	1.3	2.4	2.1
aug-cc-pVTZ	har	VSCF-PT2(cart)	VSCF-PT2(int)	exp	%err(har)	%err(anh) cart	%err(anh) int
asym str ν3	3851	3837	3777	3756	2.5	2.2	0.6
sym str ν1	3723	3712	3663	3657	1.8	1.5	0.2
bend ν2	1652	1583	1598	1595	3.6	0.8	0.2
Water Dimer							
6-31G(d,p)	har	VSCF-PT2(cart)	VSCF-PT2(int)	exp	%err(har)	% err(anh) cart	%err(anh) int
acc ν3	4010	3700	3860	3745	7.1	1.2	3.1
donor ν3	4001	3725	3851	3735	7.1	0.3	3.1
acc ν1	3878	3635	3714	3660	6.0	0.7	1.5
donor ν1	3819	3564	3689	3601	6.1	1.0	2.5
donor ν2	1713	1671	1668	1616	6.0	3.4	3.2
acc ν2	1678	1596	1652	1599	5.0	0.2	3.3
OPB	665	742	535	523	27.1	41.9	2.3
IPB	429	589	178	311	38.0	89.4	42.9
S	204	161	182	143	42.5	12.5	27.2
AT	162	434	113	108	49.9	301.7	4.9
AW	144	313	130	103	39.9	203.9	25.9
DT	89	396	108	88	1.6	349.6	22.8
aug-cc-pVDZ	har	VSCF-PT2(cart)	VSCF-PT2(int)	exp	%err(har)	% err(anh) cart	%err(anh) int
acc ν3	3925	3624	3801	3745	4.8	3.2	1.5
donor ν3	3905	3667	3747	3735	4.5	1.8	0.3
acc ν1	3796	3553	3629	3660	3.7	2.9	0.9
donor ν1	3705	3466	3578	3601	2.9	3.8	0.6
donor ν2	1643	1598	1598	1616	1.6	1.1	1.1
acc ν2	1624	1557	1598	1599	1.6	2.7	0.1
OPB	639	733	483	523	22.2	40.0	7.5
IPB	357	544	289	311	14.9	75.0	7.2
S	184	163	192	143	28.3	14.1	34.1
AT	150	420	122	108	39.2	289.0	12.6
AW	148	325	127	103	43.3	215.3	23.1
DT	128	431	91	88	45.0	389.7	3.1

Table VI. MP2/aug-cc-pVDZ thermodynamic properties for the water dimerization reaction at T=373K and P=1bar.

Thermodynamic property	har	VSCF-PT2 (cart)	VSCF-PT2 (int)	Expt.
ΔH (kcal/(mol•K))	-3.42	-3.11	-3.27	-3.59±0.5[a]
ΔS (cal/(mol•K))	-19.71	-25.85	-17.68	-18.59±1.30[a]
K_p(atm^{-1})	0.0050	0.0001	0.0113	0.0064[b] 0.0110[a] 0.0160[c]

[a]Estimated from thermal conductivity measurements by Curtiss *et al.* (Ref. [59]).

[b] $K_p \simeq 0.0293 \frac{e^{D_0/kT} - 1}{T}$, where D_0=3.27kcal/mol as fitted to thermodynamic data by Evans and Vaida (Ref. [61]).

[c] $K_p = -(B - b_0)/RT$ where B(373K)=452.3 cm^3/mol was determined by Harvey and Lemmon (Ref. [60]) and b_0=38.5 cm^3/mol was estimated by Curtiss *et al.* (Ref. [59]).

Table VII. MP2/6-31G(d,p) vibrational frequencies of H_2SO_4 and urea molecules. Experimental values are taken from Ref. [18].

H_2SO_4							
mode	har	VSCF-PT2 cart	VSCF-PT2 int	exp	%err(har)	%err(anh) cart	%err(anh) int
1	3825	3575	3660	3567	7.2	0.2	2.6
2	3820	3488	3653	3563	7.2	2.1	2.5
3	1491	1467	1471	1452	2.7	1.0	1.3
4	1228	1214	1212	1216	1.0	0.2	0.3
5	1189	1139	1164	1157	2.8	1.6	0.6
6	1172	1118	1131	1136	3.2	1.6	0.4
7	873	855	860	882	1.0	3.1	2.5
8	810	797	797	831	2.5	4.1	4.1
9	529	543	528	558	5.2	2.7	5.4
10	527	521	527	548	3.8	4.9	3.8
11	477	451	473	506	5.7	10.9	6.5
12	428	429	393	422	1.4	1.7	6.9
13	358	351	341	379	5.5	7.4	10.0
14	312	350	262	288	8.3	21.5	9.0
15	240	53	216	224	7.1	76.3	3.6
urea							
mode	har	VSCF-PT2 cart	VSCF-PT2 int	exp	%err(har)	%err(anh) cart	%err(anh) int
24	3790	3597	3715	3545	6.9	1.5	4.8
23	3790	3585	3714	3535	7.2	1.4	5.1
22	3662	3469	3528	3440	6.4	0.8	2.6
21	3659	3468	3589	3440	6.4	0.8	4.3
20	1866	1832	1840	1740	7.2	5.3	5.7
19	1677	1635	1722	1590	5.5	2.8	8.3
18	1667	1656	1651	1590	4.8	4.2	3.8
17	1454	1420	1425	1393	4.4	2.0	2.3
16	1205	1192	1184	1145	5.2	4.1	3.4
15	1084	1079	1051	1004	7.9	7.5	4.7
14	972	957	950	940	3.5	1.8	1.1
13	794	809	795	785	1.1	3.1	1.3
12	649	695	593	580	11.9	19.9	2.2
11	595	684	642	555	7.3	23.3	15.7
10	560	553	554	543	3.1	1.9	2.0
9	476	485	482	500	4.8	3.0	3.5
8	458	516	455	479	4.5	7.7	5.1
7	409	291	388	233	75.7	24.7	66.5

Appendix

Appendix A. Dependence of entropy on frequency

$$S_{vib} = -R\sum_{i}^{f} \ln(1 - e^{-h\nu_i / kT}) + R\sum_{i}^{f} \frac{h\nu_i}{kT} \frac{e^{-h\nu_i / kT}}{(1 - e^{-h\nu_i / kT})}$$

The first term is:

$$-\ln(1 - e^{-c\nu_i}) = \ln \frac{1}{1 - e^{-c\nu_i}} = \ln \frac{e^{c\nu_i}}{e^{c\nu_i} - 1} = c\nu_i - \ln(e^{c\nu_i} - 1) = c\nu_i + \ln \frac{1}{e^{c\nu_i} - 1} \quad ,$$

while the second term gives:

$$c\nu_i \frac{e^{-c\nu_i}}{1 - e^{-c\nu_i}} = c\nu_i \frac{1}{e^{c\nu_i} - 1}, \text{ where } c = h / kT \, .$$

So, both terms are decreasing while frequency increases.

Appendix B. Heat capacity (C_p^0) data

Table VIII shows heat capacity (C_p^0) data

Table VIII. Heat capacity (cal/(mol*K) [δ(anh-cal)=$\Delta C_p^0{}_{anh}$-$\Delta C_p^0{}_{cal(expfreq)}$; δ(har-anh)= $\Delta C_p^0{}_{har}$-$\Delta C_p^0{}_{anh}$; δ(har-exp)= $\Delta C_p^0{}_{har}$-$\Delta C_p^0{}_{exp}$; δ(anh-exp)= $\Delta C_p^0{}_{anh}$-$\Delta C_p^0{}_{exp}$; δ(cal-exp)= $\Delta C_p^0{}_{cal(expfreq)}$-$\Delta C_p^0{}_{exp}$] calculated using the harmonic formula with: harmonic ($\Delta C_p^0{}_{har}$), anharmonic ($\Delta C_p^0{}_{anh}$) and experimental frequencies ($\Delta C_p^0{}_{cal(expfreq)}$). Experimental frequencies are taken from Ref. [18], except diatomic molecules (Ref. [50]), $(HF)_2$ (Ref. [66]), and $(H_2O)_2$ (Ref. [67]). Experimental entropy is $\Delta C_p^0{}_{exp}$. Experimental data are taken from Ref. [18], except for Br_2 and I_2 which are taken from Ref. [71], and H_2O_2 (Ref. [50]).

Molecule	$\Delta C_p^0{}_{har}$	$\Delta C_p^0{}_{anh}$	$\Delta C_p^0{}_{cal(expfreq)}$	$\Delta C_p^0{}_{exp}$ [4]	δ(anh-cal)	δ(har-anh)	δ(har-exp)	δ(anh-exp)	δ(cal-exp)
H_2[a]	6.96	6.96	6.96	6.89	0.00	0.00	0.07	0.07	0.07
H_2[c]	6.96	6.96	6.96	6.89	0.00	0.00	0.07	0.07	0.07
HF[a]	6.96	6.96	6.96	6.96	0.00	0.00	0.00	0.00	0.00
HF[c]	6.96	6.96	6.96	6.96	0.00	0.00	0.00	0.00	0.00
F_2[a]	7.34	7.36	7.47	7.48	-0.11	-0.02	-0.14	-0.12	-0.02
F_2[b]	7.33	7.35	7.47	7.48	-0.12	-0.02	-0.15	-0.13	-0.02
F_2[c]	7.43	7.47	7.47	7.48	0.00	-0.03	-0.05	-0.01	-0.02
Cl_2[a]	8.11	8.13	8.08	8.11	0.04	-0.01	0.00	0.02	-0.03
Br_2[a]	8.57	8.58	8.58	8.61	-0.01	0.00	-0.04	-0.04	-0.03
I_2[d]	8.75	8.75	8.77	8.82	-0.02	0.00	-0.07	-0.07	-0.05
H_2O[a]	7.99	8.00	8.00	8.03	0.00	-0.01	-0.04	-0.03	-0.03
NH_3[a]	8.28	8.41	8.48	8.52	-0.07	-0.13	-0.24	-0.11	-0.04
CH_4[a]	8.36	8.43	8.52	8.53	-0.09	-0.07	-0.17	-0.10	-0.01
H_2O_2[a]	10.26	10.39	10.28	10.29	0.11	-0.14	-0.03	0.10	-0.01
H_2S_2[a]	11.36	11.52	11.66	11.76	-0.14	-0.16	-0.40	-0.24	-0.10
H_2SO_4[a]	19.90	20.21	19.78	20.17	0.43	-0.32	-0.27	0.04	-0.39
CH_3NO_2[a]	14.38	14.28				0.10			
urea[a]	16.89	16.75	17.63	17.09	-0.88	0.14	-0.20	-0.34	0.54
$(HF)_2$[e]	14.22	12.66	14.54	13.89	-1.89	1.57	0.33	-1.23	0.65
$(H_2O)_2$[a]	17.92	16.26	18.64		-2.38	1.65			
$(H_2O)_6$[a]	51.61	45.06				6.55			
$(H_3Si)_2O$[a]	20.21	20.13				0.08			
$((HO)_2HSi)_2O$[a]	36.32	35.23				1.09			
$(H_2SiO)_3$[a]	29.21	29.02				0.18			
$(H_2SiO)_4$[a]	40.16	39.91				0.25			

Level of theory/basis set: [a]MP2/6-31G(d,p); [b]MP2/aug-cc-pVTZ; [c]CCSD(T)/aug-cc-pVTZ; [d]MP2/midi; [e]MP2/p-TZV with diffuse functions.

CHAPTER 3. PREDICTING ACCURATE VIBRATIONAL FREQUENCIES FOR HIGHLY ANHARMONIC SYSTEMS

Bosiljka Njegic and Mark S. Gordon

Abstract

Improvements in the manner in which the potential energy surface (PES) is generated in the vibrational self-consistent field (VSCF) method have been implemented. The PES can now be computed over a flexible range of displacements and in internal rather than Cartesian coordinate space, leading to higher accuracy of the calculated vibrational frequencies. The coarse-grained parallelization of the PES calculations, which is computationally by far the most expensive part of the VSCF method, enables the usage of higher levels of theory and larger basis sets. The new VSCF procedure is discussed and applied to three examples, H_3^+, HNO_2 and HNO_3, to illustrate its accuracy and applicability.

1. Introduction

Experimental vibrational spectra can be sufficiently complex that computational guidance is essential for interpretation. The importance of accurate calculated vibrational frequencies extends to the prediction of thermodynamic and kinetic properties that depend on the construction of the appropriate partition functions.

Vibrational frequencies may be calculated at several levels of theory. The computationally least demanding approach is a normal mode analysis based on the second order derivatives of the energy obtained most commonly from some level of electronic structure theory. This approach provides uncoupled harmonic vibrational frequencies. To improve the accuracy of calculated frequencies one can use scaling factors that are obtained by fitting the harmonic frequencies to experimental data for a modest subset of molecules[1]. These scaling factors have been determined for several levels of theory and basis sets. Scaling harmonic frequencies has often worked well; however, using a single scale factor for a full range of vibrations, from stiff stretching modes to large amplitude torsions or intermolecular vibrations, can be problematic, since high frequency modes are more likely to be harmonic. In addition, a more sophisticated approach is required to predict the details of a vibrational spectrum.

In order to achieve accurate predictions of vibrational spectra, a reliable level of electronic structure theory and an accurate analysis of the potential energy surface (PES) are needed in order to determine the vibrational energy levels and to account for both the anharmonicity and the coupling of the molecular vibrations. In the present work, the latter is accomplished with the vibrational self-consistent field (VSCF) method[2,3], developed in the late 1970s[4-7].

In the VSCF approach, the PES is generally calculated on a grid, since analytic expressions are not available. This is computationally very expensive, because of the large number of PES points that are required, often at a high level of electronic structure theory. Such an investment of computer time demands both

accuracy and efficiency. Therefore, the PES is evaluated at a relatively small number of points that must be chosen carefully, since the accuracy of the calculated vibrational frequencies depends on how well these points capture the anharmonicity and the coupling of molecular vibrations. The manner in which the PES is generated is revised and parallelized in the present work.

2. Computational Details

Calculations were performed using the cc-pVDZ and cc-pVTZ basis sets[8] for the H_3^+, HNO_2 and HNO_3 molecules. Second order perturbation theory (MP2[9-11]) was used for all three molecules. The most accurate calculations were done at the coupled cluster level of theory. The CCSD[12,13] (coupled cluster with singles and doubles) method was used for H_3^+ and CCSD(T)[13,14], which adds perturbative triples, was employed for HNO_2 and HNO_3.

Molecules in their appropriate symmetries, shown in Fig. 1, were tightly optimized[15-17] with the largest component of the gradient being less than $1x10^{-5}$ Hartree/Bohr. Coupled cluster geometry optimizations were achieved using numerical gradients.

Hessian[18] (matrix of energy second derivatives) calculations were performed at the optimized geometries. Minima on each potential energy surface were established by confirming that the corresponding Hessian is positive definite. Semi-numerical MP2 Hessians were obtained using double differencing of analytic gradients, while fully numerical Hessians were used in the coupled cluster calculations. Improved harmonic vibrational frequencies are obtained by scaling of

the harmonic frequencies. Scaling factors were taken from the NIST database[19]: 0.950 MP2/ccd, 0.936 MP2/cct, 0.947 CCSD/ccd, 0.941 CCSD/cct, 0.979 CCSD(T)/ccd and 0.975 for CCSD(T)/cct.

The vibrational self-consistent field method (VSCF) was used to calculate anharmonic and coupled vibrational frequencies. The VSCF method consists of two computationally independent parts: generating the PES on the grid, and calculating the vibrational energy levels. An overview of the VSCF method is presented here. Specific details about the manner in which the PES was generated can be found in the following section.

Two important sets of data are provided by Hessian calculations that guide the construction of a PES on the grid. The normal mode displacement vectors designate the direction in which the displacements from the equilibrium geometry will be made. The spacing of the displacements along the normal mode is based on the magnitude of the corresponding harmonic frequency and a factor that was chosen so that the wave function tails are always within the chosen maximum displacement along normal modes[20,21]. In particular, starting from the equilibrium structure, eight displacements are made in both the positive and the negative direction of each normal mode displacement vector. Thus, a total of 16 structures (points on the PES) are generated for each normal mode. These structures (and energies) comprise the necessary information for determining the anharmonicity associated with each normal mode. Single point energy calculations performed at these 16 points generates the “diagonal potential”, which captures the anharmonicity along the normal mode.

In order to gather information about coupling of the vibrations, simultaneous displacements along two (or more) normal modes is required. This gives rise to a 16x16 grid of points for each pair of vibrations. Single point energy calculations are then performed on these grids, generating the coupling potential, which accounts for the coupling of the vibrations.

Once the PES is created as described above, vibrational energy level calculations are then performed at three levels of theory. The diagonal vibrational frequencies are always calculated, but they are generally not sufficiently acurate. Although they do account for the anharmonicity in the individual vibrational modes, the coupling is neglected since only the diagonal potential is used to calculate them. Vibrational self-consistent field calculations are then performed in which coupling is included through a mean field approximation. Finally, a second order perturbation theory correction is used to achieve more accurate vibrational frequencies.

All calculations described here were carried out using the GAMESS program suite[20,21] and molecules were visualized with the MacMolPlot program[22]. Some calculations were carried out in parallel on two types of clusters: An IBM pSeries Cluster with 32 quad-processor nodes and an IBM BlueGene/L ("CyBlue") with 1024 dual-core nodes. The calculations on CyBlue were run in co-processor mode, so only one processor per node was performing the computations.

3. Results and Discussion

Various aspects of the new VSCF method developments are discussed in the following paragraphs. The spacing of the PES points is considered in Section 3.1,

while Section 3.2 addresses the manner in which the displacements are made. The parallelization of the PES calculations is presented in Section 3.3.

3.1. Adaptive grid of the PES points

The PES is generated on a grid by making displacements from the equilibrium geometry along normal modes (diagonal potential) and pairs of normal modes (coupling potential). In the standard implementation of the VSCF method[2,3], the range of the PES points is based on the magnitude of the harmonic frequencies:

$$Q_i(amp) = \frac{4}{\sqrt{\nu_i}}, \qquad \text{Eq. 1}$$

where Q_i(amp) is the maximum displacement expressed in normal mode coordinates taken along the i^{th} normal mode, and ν_i is the frequency of the i^{th} mode. The factor of 2 is chosen to ensure that the wave function will decay to zero upon reaching the furthest points (classical turning points) along the normal modes. This will be discussed further below.

The starting point in the VSCF procedure is still a normal mode analysis. Although a normal mode analysis provides normalized normal mode amplitudes, rather then their absolute values, the absolute values of the amplitudes can be calculated as follows. The vibrational energy of the n^{th} energy level for the i^{th} normal mode $E_i^{(n_i)}$, is given by:

$$E_i^{(n_i)} = \left(n_i + \frac{1}{2}\right) h\nu_i, \qquad \text{Eq. 2}$$

where n_i=0,1,2,…, h is Planck's constant, and ν_i is the fundamental frequency of the i^{th} normal mode.

At the classical turning points, the (classical) kinetic energy is zero, and the vibrational energy is all potential energy:

$$E_i^{(n_i)} = \frac{1}{2} k_i \left(A_i^{(n_i)} \right)^2 , \qquad \text{Eq. 3}$$

where k_i is the force constant and $A_i^{(n_i)}$ is the amplitude of the displacement for the n^{th} energy level of the i^{th} mode.

Combining Eq. 1 and 2 yields the following expression:

$$\left(n_i + \frac{1}{2} \right) h\nu_i = \frac{1}{2} k_i \left(A_i^{(n_i)} \right)^2 , \qquad \text{Eq. 4}$$

After substituting $k_i = 4\pi^2 m_i \nu_i^2$ and rearrangement, the amplitude of the displacement can be expressed as:

$$A_i^{(n_i)} = \sqrt{\frac{\left(n_i + \frac{1}{2} \right) h}{2\pi^2 m_i \nu_i}} , \qquad \text{Eq. 5}$$

By analogy with Eq. 5, the amplitude of normal mode displacement ($Q_i^{(n_i)}(amp)$) may be postulated as:

$$Q_i^{(n_i)}(amp) = \sqrt{\frac{2\left(n_i + \frac{1}{2} \right)}{\nu_i}} , \qquad \text{Eq. 6}$$

since m=1 in mass-weighted coordinates and since $\frac{h}{2\pi} = 1$ in atomic units.

For n_i=7.5, Eq. 6 becomes:

$$Q_i^{(n_i=7.5)}(amp) = \frac{4}{\sqrt{\nu_i}}, \qquad \text{Eq. 7}$$

which recovers Eq. 1 as a special case of Eq. 6.

Eq. 6 can be used to determine the range of the PES points in the VSCF method. $Q_i^{(n_i)}(amp)$ is the total displacement to be taken from the equilibrium geometry, following the normal mode vector in the positive and negative directions. This determines, along each normal mode, the two extreme displacement points from the equilibrium geometry. The remaining points are spaced equidistantly between these two points.

Since the number of points is constant along the mode, increasing the value of n_i increases the range as well. Although n_i is an integer in the harmonic approximation, once anharmonicity is introduced, the energy levels are no longer equidistant. Consequently, n_i no longer needs to be an integer. This facilitates the possibility of additional fine-tuning of the VSCF calculation.

The affect of the spacing (range) of the PES points on the accuracy of the VSCF method can be illustrated by calculations carried out on H_3^+, summarized in Table 1. Diagonal frequencies are calculated as a function of n_i. As n_i increases the diagonal frequencies decrease, and ultimately converge to constant values. At this point, any further increase in the covered PES area is not useful. Typically, higher vibrational frequencies larger values of n_i to reach convergence.

In order to minimize the computational cost, it is recommended to use the diagonal potential to determine the value of n_i for which frequencies are converged.

Once the optimal value of n_i is determined, the full PES (diagonal + coupling potential) should be recalculated using n_i+1.

3.2. Internal vs. Cartesian Normal Mode Displacement Vectors

The normal mode displacement vectors are commonly expressed in Cartesian coordinates. It has been shown previously[23,24] that this choice, when used to create a PES, can produce unreliable frequencies for strongly anharmonic vibrational motions. An alternative approach is to generate the PES by using normal mode displacement vectors expressed in internal, as opposed to Cartesian, coordinates. This can be achieved by decomposing normal mode displacement vectors into internal coordinates[25]. The energy calculation requires the transformation from internal to Cartesian coordinates at the chosen PES points. In the previous implementation only simple internals were used, and a rigorous mathematical procedure for direct conversion from internal to Cartesian coordinates was employed. However, other types of vibrations, such as atom-out-of-the-plane (OPLA), require an iterative procedure adopted from the work of Pulay et al.[26] to transform the coordinates. The iterative procedure fails when large steps are taken along the PES. This is remedied by using the current point to determine the next point on the PES. This ensures that displacements are as small as possible, thereby enabling the convergence of the coordinate transformation.

3.2.1. Recommended Procedure

The combination of generating the PES in internal coordinates with the flexible spacing of the points provides an effective procedure for conducting VSCF calculations. The flow chart presented in Figure 2 lists three important steps in the procedure. The first step is a preliminary VSCF calculation and should therefore be conducted at the lowest computational cost.

The first step is concerned with the selection of the internal coordinates. This step is omitted if the PES is being generated in Cartesian coordinates. However, if the PES is generated in internal coordinates it is crucial to find the set of internal coordinates that properly captures the vibrational motions. Since the choice of internal coordinates is not unique, it might be necessary to try several different combinations of internal coordinates. Since the selection of the most appropriate internals is independent of the level of theory and basis set, the most cost-efficient electronic structure method should be used.

The next important task is to find the optimal spacing between the PES points. Step 2 should be carried out at the desired level of theory and basis set, since the convergence of calculated frequencies may be method and/or basis set dependent.

Upon the successful completion of the previous steps, the actual VSCF calculation takes place, yielding anharmonic vibrational frequencies (Step 3). At this point, both diagonal and coupling potentials are generated at the desired level of theory and basis set and used to calculate the vibrational energy levels.

Three examples were chosen to illustrate the accuracy and applicability of the new approach. The H_3^+, HNO_2 and HNO_3 anharmonic frequencies, which were calculated using a PES that was generated in internal coordinates, are compared below to the harmonic, scaled harmonic and anharmonic frequencies obtained from a PES generated in Cartesian coordinates, as well as with available experimental data, taken from NIST database[19] if not stated otherwise.

3.2.2. H_3^+

Since H_3^+ is a triatomic molecule (Figure 1), the choice of internal coordinates is limited to two possibilities: two bonds and an angle, or three bonds (Figure 2, Step 1). H_3^+ has D_{3h} symmetry, suggesting that the best choice might be three bonds. To test this, calculations were performed using both sets of internals. The results are presented in Table 2 in columns labeled as anhr(int)-3b (three bonds) and anhr(int)-2ba (two bonds and an angle). The combination of two bonds and an angle removes the degeneracy of the deformation mode, giving rise to two frequencies that differ by more than 300 cm^{-1} with MP2/ccd, and more than 500 cm^{-1} using MP2/cct. Although these differences decrease to less than 50 cm^{-1} when CCSD is used, the degeneracy is still lost, making this choice of internal coordinates unacceptable. Even if the PES is constructed using normal mode displacement vectors decomposed into three bonds, these two modes differ by ~35 cm^{-1} at the MP2 level of theory, very likely due to numerical round-off. When three bonds are chosen and CCSD is employed, the degeneracy of this mode is preserved.

Upon successful selection of the internal coordinates, the optimal spacing between PES points was determined by increasing the range until the convergence of the diagonal vibrational frequencies was attained (See Figure 2, Step 2 and Table 1). The frequencies shown in bold in Table 1 have been converged and the corresponding ranges were used in the subsequent calculations (See Figure 2, Step 3).

The coupled and anharmonic vibrational frequencies were calculated (Figure 2, Step 3) with MP2/cc-pVDZ, MP2/cc-pVTZ, and CCSD with the cc-pVDZ, cc-pVTZ, and cc-pVQZ basis sets (Table 2). One can see significant basis set dependencies among the calculated vibrational frequencies shown in Table 2. Changes on the order of 100 cm^{-1} are observed upon improving the basis set from cc-pVDZ to cc-pVZT at both the MP2 and CCSD levels of theory. The changes in calculated frequencies are negligible as the basis set is improved from cc-pVTZ to cc-pVQZ at the CCSD level of theory. This means that the CCSD errors using the cc-pVQZ or cc-pVTZ basis sets define the accuracy of the VSCF method for H_3^+. The errors for various levels of theory are summarized in Table 3.

Focusing on the CCSD/cc-pVTZ frequencies, the absolute error for harmonic frequencies is ~250 cm^{-1}, while scaling of the harmonic frequencies significantly lowers the error to 50–80 cm^{-1}. Anharmonic frequencies obtained using Cartesian coordinates are inconsistent, providing high accuracy for the highest vibrational mode (an error of 3 cm^{-1}) while the degenerate mode has an error of ~90 cm^{-1}. On the other hand, the anharmonic frequencies obtained using internals are in excellent agreement with experiment[27,28], within 20 cm^{-1}. Furthermore, VSCF in internals is the

only approach that gives reliable predictions for the combination and first overtone frequencies, to within ~30 cm^{-1} of the experimental values. The second overtone is predicted with a lower accuracy of ~150 cm^{-1}. However, this is still more accurate than harmonic (error~800 cm^{-1}), scaled harmonic (error ~300 cm^{-1}) or anharmonic in Cartesian coordinates (error~850 cm^{-1}).

There is a very nice review by Jaquet[29] on first-principles studies of the rotovibrational spectra of H_3^+. Different types of fitted potentials[30-32] were used, yielding fundamentals, the $\nu_1\nu_2$ combination band, and the $2\nu_2$ and $3\nu_2$ overtones with an accuracy of less then 1 cm^{-1}. The most accurate calculations performed in the current work, at the CCSD/ccq level of electronic structure theory and using the VSCF method in internal coordinates, have an accuracy of ~20 cm^{-1} for fundamentals and ~30 cm^{-1} for the combination band and the $2\nu_2$ overtone. The source of the remaining error may be the need for a higher level of electronic structure theory, mode-mode coupling beyond pairwise interations, and/or the need to explicitly express the vibrational Hamiltonian in internal coordinates.

3.2.3. HNO_2

Now, consider HNO_2, whose vibrational motions can be described using simple internal coordinates, such as bond stretching, angle bending and torsion as depicted in Figure 1 and summarized in Tables 4 and 5. The calculations were performed with MP2 and CCSD(T), using the cc-pVDZ and cc-pVTZ basis sets. Harmonic and scaled harmonic frequencies have the same low accuracy (Table 4),

with the highest absolute error being ~200 cm^{-1} and ~120 cm^{-1}, respectively, independent of the basis set or the level of theory.

Anharmonic vibrational frequencies obtained using normal mode displacements in Cartesian coordinates have the largest absolute errors, in the range of ~50 cm^{-1} for MP2 and ~70 cm^{-1} for CCSD(T). On the other hand, generating the PES by following the normal mode displacement vectors in internal coordinates, the absolute errors decrease from ~45 cm^{-1} with MP2 to less than 30 cm^{-1} with CCSD(T).

In order to determine the origin of the difference in predicted vibrational frequencies, depending on the choice of the coordinates, consider the PES generated along the modes and the coupling potential more closely. Diagonal and VSCF (without PT2 correction) frequencies calculated with CCSD(T) using the cc-pVDZ basis set are listed in Table 5. First, consider the differences in diagonal frequencies obtained using Cartesian (diag(cart)) and internal coordinates (diag(int)). The largest differences are found for the torsional mode ν_6, and a somewhat smaller difference for the ν_3 bending mode. These two modes are not adequately described in Cartesian coordinate space. Now, by comparison of diagonal (diag(cart) and diag(int)) and frequencies calculated with coupling (vscf(cart) and vscf(int)), the magnitude of the coupling can be estimated. These differences are listed in Table 5 as diff(cart) and diff(int) for the PES generated in Cartesian or internal coordinates, respectively. There is a weak coupling of the modes calculated using internal coordinates with diff(int) less than 20 cm^{-1}. On the other hand, calculations carried out in Cartesian coordinates exhibit a significant change of 100-200 cm^{-1} in the

values of vscf(cart) compared to diag(cart) (Table 5 diff(cart)). These inconsistencies are due to the improper description of the torsional and bending motions in HNO_2 when Cartesian normal mode displacement vectors are used to generate the PES. Thus, the errors in generating the PES along these two modes are propagated when the coupling is taken into consideration, affecting now three modes: ν_{12}, ν_{10} and ν_6, due to strong coupling.

Figure 3 illustrates the choice of coordinate system on the PES by plotting the O2-H1 bond stretch against the O4-N3-O2-H1 torsion for mode ν_6 (Figure 3a), and against the N3-O2-H1 bend for mode ν_3 (Figure 3b). The PES calculated using Cartesian coordinates shows significant bond stretching from 0.966Å to 1.244 Å in the torsion mode ν_6 and to 1.082Å in the bending mode ν_3. This stretching of the O-H bond distance introduces an artificial coupling of modes ν_6 and ν_3 with the OH stretching mode ν_1, leading to a lowering of the frequencies for all three modes after the coupling. The proper description of modes ν_6 and ν_3 is accomplished by using internal coordinates, which preserve the correct O-H bond distance while allowing for the change in the torsion and bending angles.

3.2.4. HNO_3

HNO_3 (structure shown in Figure 1) provides a good test of the use of less common types of internal coordinates, such as the movement of the N atom out of the plane of the three O atoms.

The differences between calculated and experimental frequencies are listed in Table 6. Both harmonic and scaled harmonic frequencies exhibit large errors that are independent of the level of theory or the basis set. The harmonic vibrational frequencies give the largest errors, ~200 cm^{-1}. Scaling of harmonic frequencies decrease the largest error to ~100 cm^{-1}.

In contrast to the harmonic calculations, accurate anharmonic vibrational frequencies do require the use of a high level of theory and a reliable basis set. Anharmonic vibrational frequencies obtained using Cartesian coordinates give the largest absolute errors of 75 cm^{-1} at CCSD(T)/cc-pVDZ, compared to MP2/ccd and MP2/cct with largest errors of 135 cm^{-1} and 177cm^{-1}, respectively. Similar basis set and level of theory dependence is observed for anharmonic frequencies in internal coordinates. The most accurate frequencies are obtained with CCSD(T)/cc-pVDZ, with the largest absolute error of 50 cm^{-1}.

As for HNO_2, the largest difference in the diagonal potentials calculated using normal mode displacement vectors in Cartesian vs. internal coordinates, occurs for the torsional mode, ν_9 (Table 5 diff(diag)~300 cm^{-1}). This mode can be described as the H5-O2-N1-O3 torsion (see Fig. 1). In order to determine the origin of this discrepancy, the H5-O2 bond distance is plotted against the H5-O2-N1-O3 torsion angle in Figure 4a. In Cartesian coordinates, there is a stretching of the H5-O2 bond length from 0.976Å to 1.262 Å, while this distance remains constant if internal coordinates are used. Somewhat surprisingly, the H-O-N bending mode, ν_4, appears to be reasonable with either type of coordinate. However, this is misleading as shown in Figure 4b, which reveals H5-O2 stretching from 0.976Å to 1.060Å for

Cartesian coordinates and negligible stretching if internals are used. Again, shown for HNO_2 (Section 3.2.3), the frequency values for modes ν_9, ν_4 and ν_1 are lowered due to artificially strong coupling, which is caused by the exaggeration of the OH stretching character in these three modes when Cartesians are used.

3.2.5. Summary

The total errors for the vibrational frequencies of all three molecules calculated at the highest level of theory using the largest basis set for the particular molecule are plotted in Figure 5. Harmonic frequencies produce the largest absolute errors, 85 cm^{-1} on average. Scaled harmonic frequencies and anharmonic frequencies in Cartesian coordinates have comparable errors, on average 36 cm^{-1} and 32 cm^{-1} respectively. Anharmonic frequencies calculated using internal coordinates give the most accurate results with average error of 15cm^{-1}.

3.3. Coarse Grained Parallelization of the PES Calculation

The single point energy and dipole derivative tensor calculations for each PES point can be carried out independently. This provides an opportunity to employ coarse grained parallelization for this part of the code. The generalized distributed data interface[33,34] (GDDI) is used to achieve two-level hierarchical parallelization. The basic idea of coarse grained parallelism is to divide the workload into smaller independent pieces (see ref. 18 for more details). This is achieved by *a priori* dividing nodes into a specified number of groups. Each group is assigned an ID number, from 0 to N-1, with N being the number of groups. If there is more than one

processor available per group, a second level of parallelism within the group can be achieved, speeding up the calculation even more.

Figure 6 illustrates the steps taken during a parallel VSCF calculation. The VSCF calculation starts in the World scope, where there is only one master. The PES is generated using coarse grained parallelization with dynamic load balancing, meaning that the workload, the PES points at which the energy still has to be calculated, is dynamically assigned to the first available group. The energy and dipole derivative tensors are calculated and immediately stored by the working group into a distributed memory array, which is allocated once for all groups. In order to permanently save the data, the group that has ID=0, as soon as it completes the calculation on the current PES point, accesses the distributed memory array, checks for any newly acquired data, and writes that data to a disk file. Once all the PES points have been calculated, the scope switches from Group to Master and the global summation of the calculated energies and dipole vectors across the masters of all the groups takes place. Once the PES calculations are done, the scope switches back from Master to World, in which the remaining VSCF calculations are completed. The initial calculation at the equilibrium geometry is also conducted in Group scope, by the group with ID=0. The reason for the latter is that a finer level of parallelism may require a smaller number of processors than the total number of available processors.

The computationally most demanding calculations for HNO_2, with CCSD(T)/cc-pVTZ, provide a good example for illustrating the need for parallel computing. The PES in Cartesian normal mode displacement vectors was carried

out in 4 groups, while the calculation in internals was run in 8 groups and subsequently 16 groups. These calculations were done on the IBM cluster described in the computational section. The speed up from 4 to 8 to 16 groups is linear, decreasing the computational time from ~16 days to less than 4 days. Another example is the series of MP2/cc-pVDZ calculations done on HNO_3. These calculations were carried out on CyBlue from 16 to up to 256 groups. Figure 7 shows the relative speed up that starts as 1 for 16 groups and double as the number of groups doubles. The speed up is excellent up to 128 groups. Between 128 and 256 groups there is a turning point, after which there is no benefit in adding more groups. Further study is needed to push the parallelization beyond 128 groups on CyBlue.

4. Conclusions

Vibrational frequencies were calculated for three small molecules: H_3^+, HNO_2 and HNO_3. MP2 and coupled cluster methods were used with the cc-pVDZ and cc-pVTZ basis sets. Four different approaches to calculating vibrational frequencies were compared: harmonic, scaled harmonic, anharmonic with the PES generated in Cartesian coordinate space, and anharmonic with the PES generated in internal coordinates. Although small improvements in the accuracy of calculated harmonic and scaled harmonic frequencies were achieved by increasing the size of the basis set and using higher levels of theory, to obtain highly accurate vibrational frequencies one needs to include anharmonicity and coupling in the calculations, as well as to generate the PES following normal mode displacement vectors in internal, rather then Cartesian coordinates. It was found that carrying out the VSCF

calculations in internal coordinates is crucial for a proper treatment of bending and torsional types of vibrational motions, especially those involving H atom. While it is clear that the coupled cluster level of theory is needed to achieve highly accurate frequencies, the importance of the basis set depends on the molecule.

The spacing and range of the PES points is a variable in the newest implementation of the VSCF method. This enables the variation of the spacing and range of points until the convergence of vibrational frequencies is reached, assuring greater accuracy of the VSCF calculation.

Finally, coarse-grained parallelization of PES calculations on the grid was implemented. The speed up is excellent for up to 128 groups for the examples chosen. This increases the applicability of the VSCF method to bigger molecules.

Acknowledgements

This work was supported by a grant from the Air Force Office of Scientific Research. The authors are grateful for many helpful discussions with Drs. Jerry Boatz, Ryan Olson, and Michael Schmidt, and Professors Benny Gerber and Lyudmilla Slipchenko. The coarse-grained parallel calculations were carried out on the Scalable Computing Laboratory IBM Power4 cluster, and on the Iowa State University BlueGene/L computer, made available via grants from the National Science Foundation (Professor S. Aluru, PI), the Iowa State University Plant Sciences Institute, and Iowa State University.

References

(1) Pople, J. A.; Scott, A. P.; Wong, M. W.; Radom, L. *Israel Journal of Chemistry* **1993**, *33*, 345.

(2) Chaban, G. M.; Jung, J. O.; Gerber, R. B. *Journal of Chemical Physics* **1999**, *111*, 1823.

(3) Yagi, K.; Hirao, K.; Taketsugu, T.; Schmidt, M. W.; Gordon, M. S. *Journal of Chemical Physics* **2004**, *121*, 1383.

(4) Bowman, J. M. *Journal of Chemical Physics* **1978**, *68*, 608.

(5) Carney, G. D. *Advances in Chemical Physics* **1978**, *37*, 305.

(6) Cohen, M.; Greita, S.; McEachran, R. P. *Chemical Physics Letters* **1979**, *60*, 445.

(7) Gerber, R. B.; Ratner, M. A. *Chemical Physics Letters* **1979**, *68*, 195.

(8) Dunning, T. H., Jr. *Journal of Chemical Physics* **1989**, *90*, 1007.

(9) Pople, J. A.; Binkley, J. S.; Seeger, R. *International Journal of Quantum Chemistry, Symposium* **1976**, *10*, 1.

(10) Frisch, M. J.; Head-Gordon, M.; Pople, J. A. *Chemical Physics Letters* **1990**, *166*, 275.

(11) Aikens, C. M.; Webb, S. P.; Bell, R. L.; Fletcher, G. D.; Schmidt, M. W.; Gordon, M. S. *Theoretical Chemistry Accounts* **2003**, *110*, 233.

(12) Purvis, G. D., III; Bartlett, R. J. *J. Journal of Chemical Physics* **1982**, *76*, 1910.

(13) Piecuch, P.; Kucharski, S. A.; Kowalski, K.; Musial, M. *Computer Physics Communications* **2002**, *149*, 71.

(14) Raghavachari, K.; Trucks, G. W.; Pople, J. A.; Head-Gordon, M. *Chemical Physics Letters* **1989**, *157*, 479.

(15) Baker, J. *Journal of Computational Chemistry* **1986**, *7*, 385.

(16) Helgaker, T. *Chemical Physics Letters* **1991**, *182*, 503.

(17) Culot, P.; Dive, G.; Nguyen, V. H.; Ghuysen, J. M. *Theoretica Chimica Acta* **1992**, *82*, 189.

(18) Gwinn, W. D. *Journal of Chemical Physics* **1971**, *55*, 477.

(19) Russell, D. J. I. *NIST Computational Chemistry Comparison and Benchmark Database, NIST Standard Reference Database Number 101*, 2005.

(20) Gordon, M. S.; Schmidt, M. W. *Theory and Applications of Computational Chemistry: The First Forty Years* **2005**, 1167.

(21) Schmidt, M. W.; Baldridge, K. K.; Boatz, J. A.; Elbert, S. T.; Gordon, M. S.; Jensen, J. H.; Koseki, S.; Matsunaga, N.; Nguyen, K. A.; et al. *Journal of Computational Chemistry* **1993**, *14*, 1347.

(22) Bode, B. M.; Gordon, M. S. *Journal of Molecular Graphics & Modelling* **1998**, *16*, 133.

(23) Horn, T. R.; Gerber, R. B.; Ratner, M. A. *Journal of Chemical Physics* **1989**, *91*, 1813.

(24) Njegic, B.; Gordon, M. S. *Journal of Chemical Physics* **2006**, *125*, 224102/1.

(25) Boatz, J. A.; Gordon, M. S. *Journal of Physical Chemistry* **1989**, *93*, 1819.

(26) Pulay, P.; Fogarasi, G.; Pang, F.; Boggs, J. E. *Journal of the American Chemical Society* **1979**, *101*, 2550.

(27) Kao, L.; Oka, T.; Miller, S.; Tennyson, J. *Astrophysical Journal, Supplement Series* **1991**, *77*, 317.

(28) Dinelli, B. M.; Neale, L.; Polyansky, O. L.; Tennyson, J. *Journal of Molecular Spectroscopy* **1997**, *181*, 142.

(29) Jaquet, R. *Spectrochimica acta. Part A, Molecular and biomolecular spectroscopy* **2002**, *58*, 691.

(30) Jaquet, R. *Chemical Physics Letters* **1999**, *302*, 27.

(31) Jaquet, R.; Cencek, W.; Kutzelnigg, W.; Rychlewski, J. *Journal of Chemical Physics* **1998**, *108*, 2837.

(32) Roehse, R.; Kutzeinigg, W.; Jaquet, R.; Klopper, W. *Journal of Chemical Physics* **1994**, *101*, 2244.

(33) Fedorov, D. G.; Olson, R. M.; Kitaura, K.; Gordon, M. S.; Koseki, S. *Journal of Computational Chemistry* **2004**, *25*, 872.

(34) Fletcher, G. D.; Schmidt, M. W.; Bode, B. M.; Gordon, M. S. *Computer Physics Communications* **2000**, *128*, 190.

Figure 1. Optimized geometries of a.) H_3^+ at CCSD level of theory with the cc-pVTZ basis set in D_{3h} symmetry; b.) HNO_2 at CCSD(T) level of theory with the cc-pVTZ basis set in C_s symmetry; c.) HNO_3 at CCSD(T) level of theory with the cc-pVDZ basis set in C_s symmetry. Geometry parameters are listed in the set of internal coordinates that were used as the basis for the decomposition of the normal mode displacement vectors. Experimental values[19] are given in parentheses.

a.)

Set of internal coordinates:

all three bonds

0.875Å

∠ 60.0º

b.)

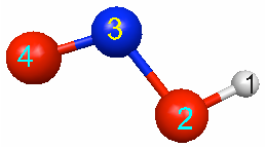

Set of internal coordinates:

r(H1-O2) = 0.966Å (0.959Å)

r(N3-O2) = 1.428Å (1.442Å)

r(O4-N3) = 1.174 Å (1.169Å)

∠(N3-O2-H1) = 101.5º (102.1º)

∠(O4-N3-O2) = 110.6º (110.6º)

∠(O4-N3-O2-H1) = 180.0º (180.0º)

c.)

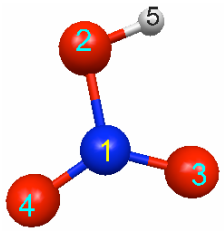

Set of internal coordinates:

r(H5-O2) = 0.976Å (0.964Å)

r(O2-N1) = 1.414Å (1.406Å)

r(O3-N1) = 1.217Å (1.211Å)

r(O4-N1) = 1.203Å (1.199Å)

∠(O3-N1-O2) = 115.5º (115.1º)

∠(O4-N1-O2) = 113.8º (113.8º)

∠(H5-O2-N1) = 101.4º (102.1º)

OPLA: N1 out of the plane of O2-O3-O4

Figure 2. Flow chart of the procedure for calculating vibrational frequencies using the VSCF method in internal coordinates. VSCF-Diagonal stands for anharmonic frequencies calculated without coupling, while VSCF-PT2 stands for anharmonic coupled vibrational frequencies calculated using a second order perturbation theory correction.

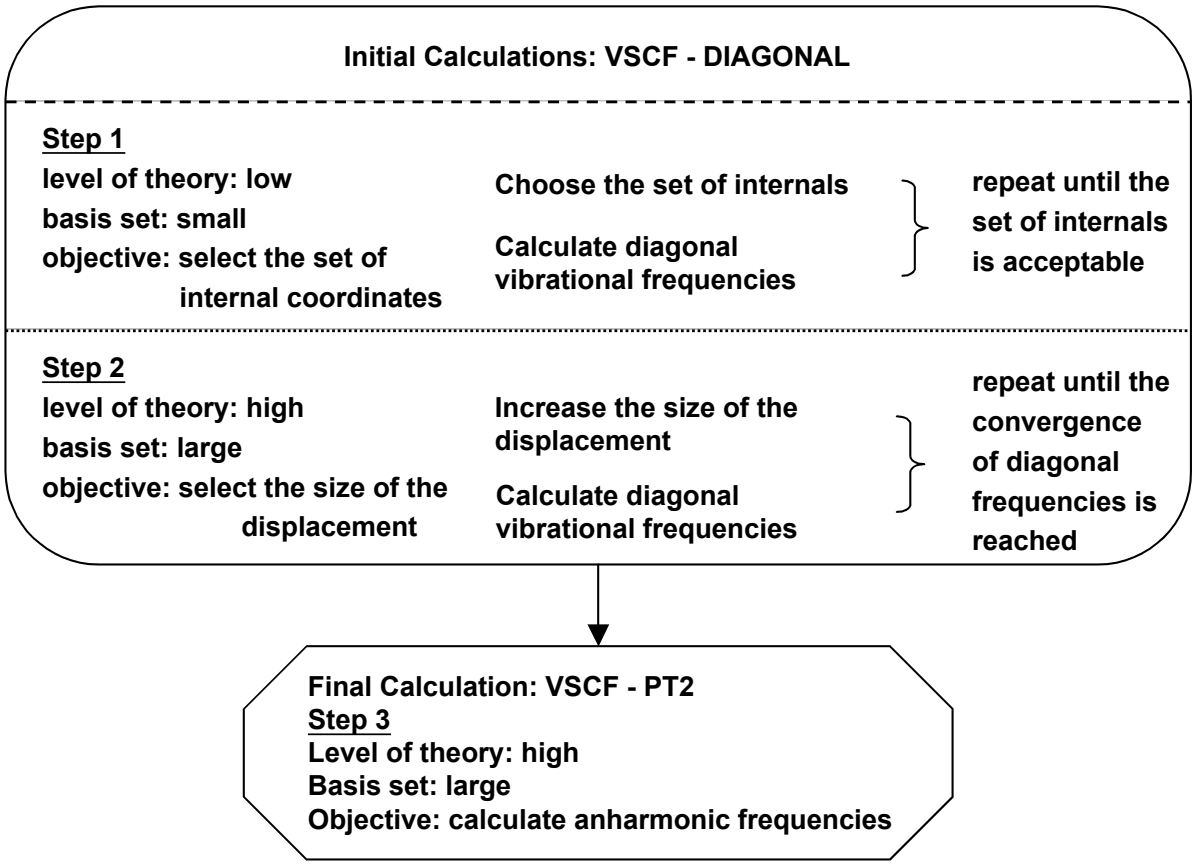

Figure 3. CCSD(T)/cc-pVTZ HNO_2 in Cartesian coordinates (dotted line) and internal coordinates (solid line). a.) H1-O2 bond distance is plotted against O4-N3-O2-H1 torsion angle at the VSCF points along the torsion mode ν_6; b.) H1-O2 bond distance is plotted against the N3-O2-H1 angle at the VSCF points along the bending mode ν_3.

a.)

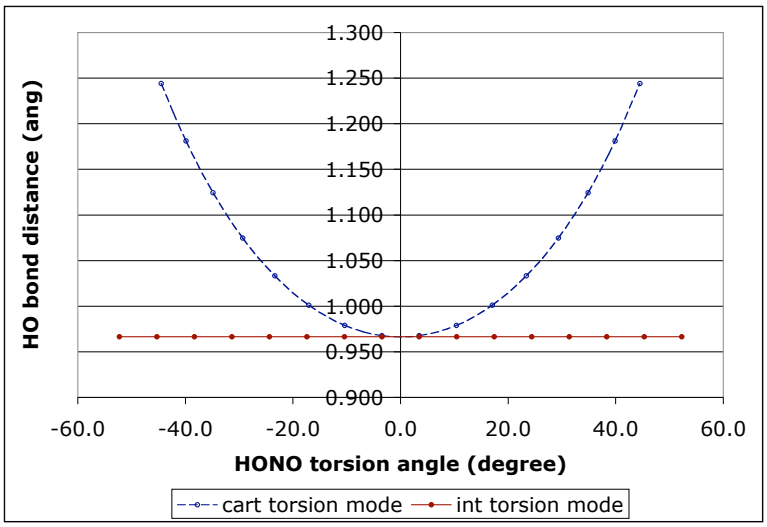

b.)

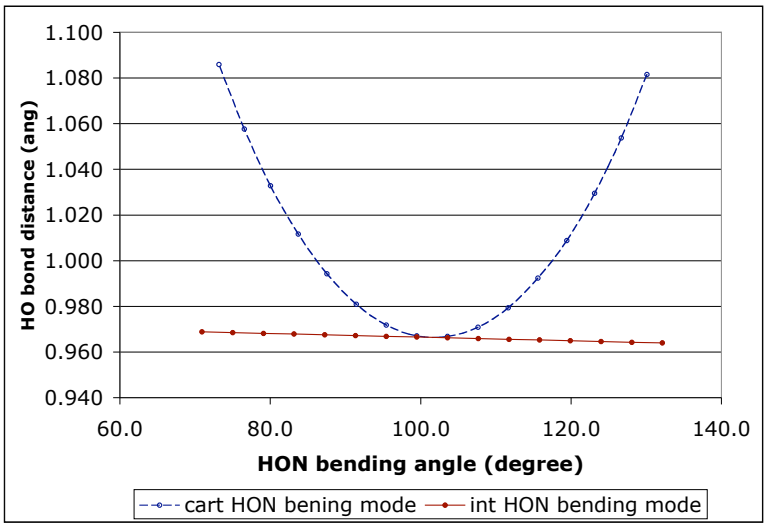

Figure 4. CCSD(T)/cc-pVDZ HNO_3 in Cartesian coordinates (dotted line) and internal coordinates (solid line). a.) H5-O2 bond distance is plotted against H5-O2-N1-O3 torsion angle at the VSCF points along torsion mode ν_9. b.) H5-O2 bond distance is plotted against H5-O2-N1 bending angle on the VSCF points along bending mode ν_4.

a.)

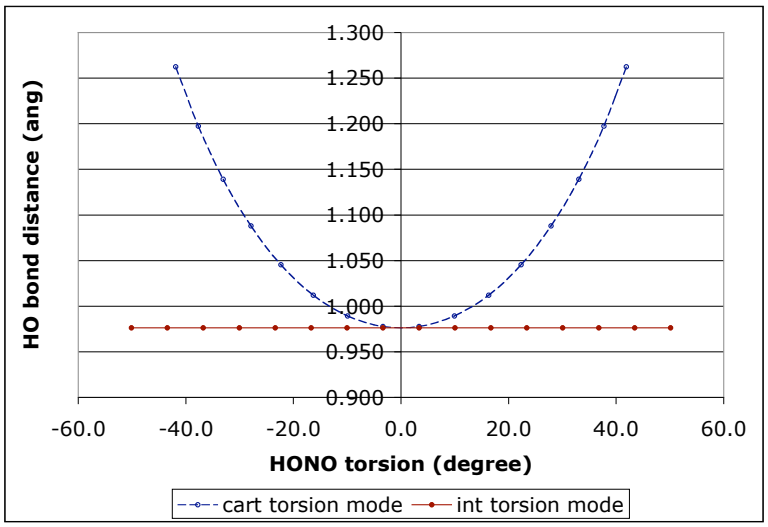

b.)

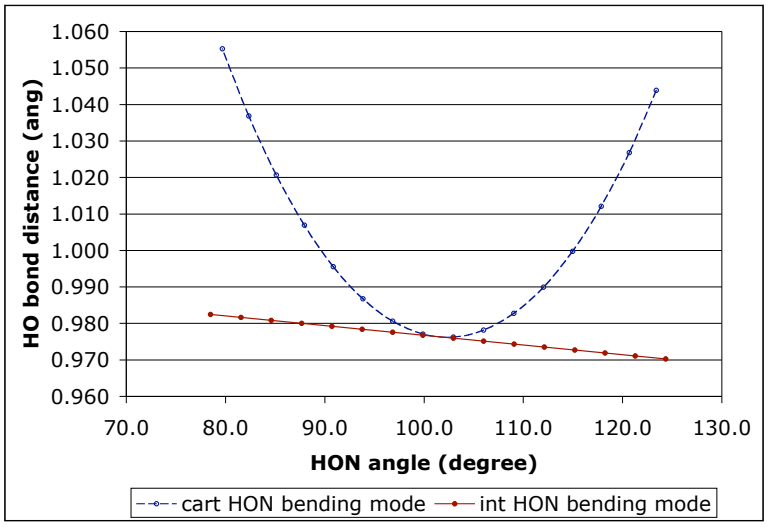

Figure 5. Total errors obtained as a difference between calculated and experimental vibrational frequencies.

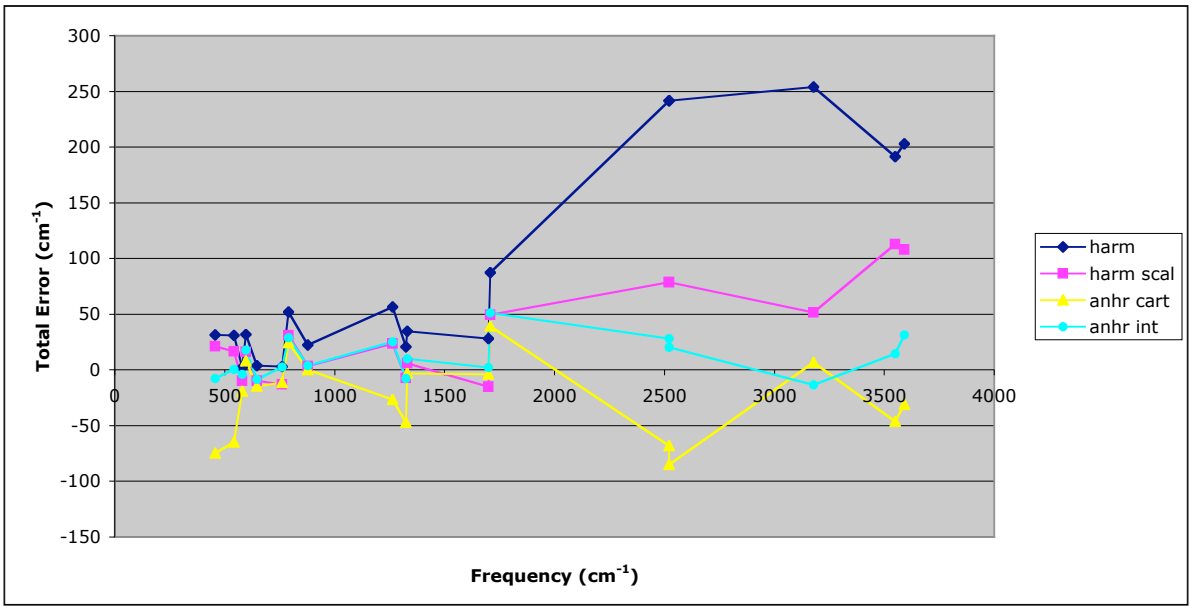

Figure 6. Coarse Grained Parallelization of PES calculations in the VSCF method.

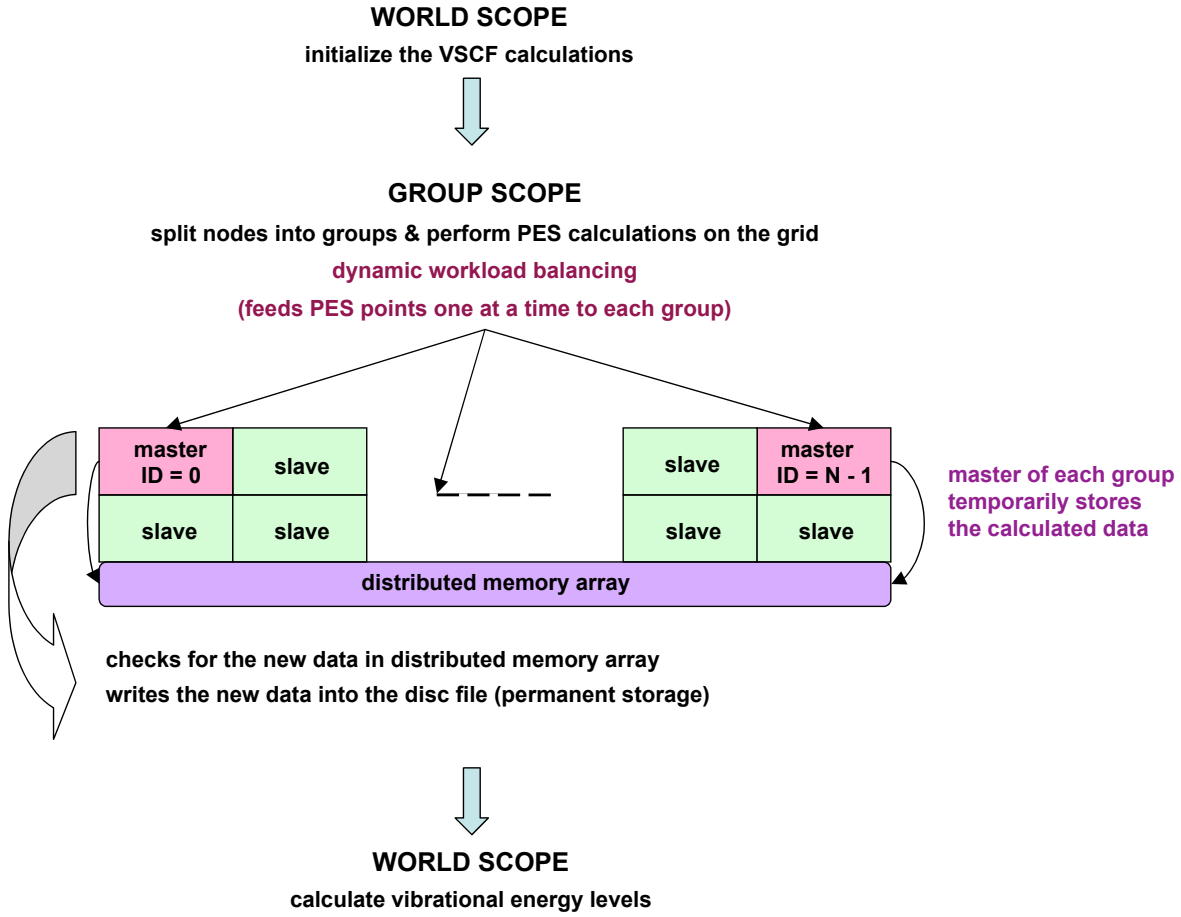

Figure 7. Speed up curve for parallelized VSCF at MP2 level of theory with the cc-pVDZ basis set carried out on HNO_3 molecule. Blue line with data point represented as triangles is the theoretical curve that follows linear speed up. The actual speed up is represented by dark red line with circles as data points. Beneath each point in parentheses are given the number of points per each group that needed to be calculated, followed up by the timings in minutes.

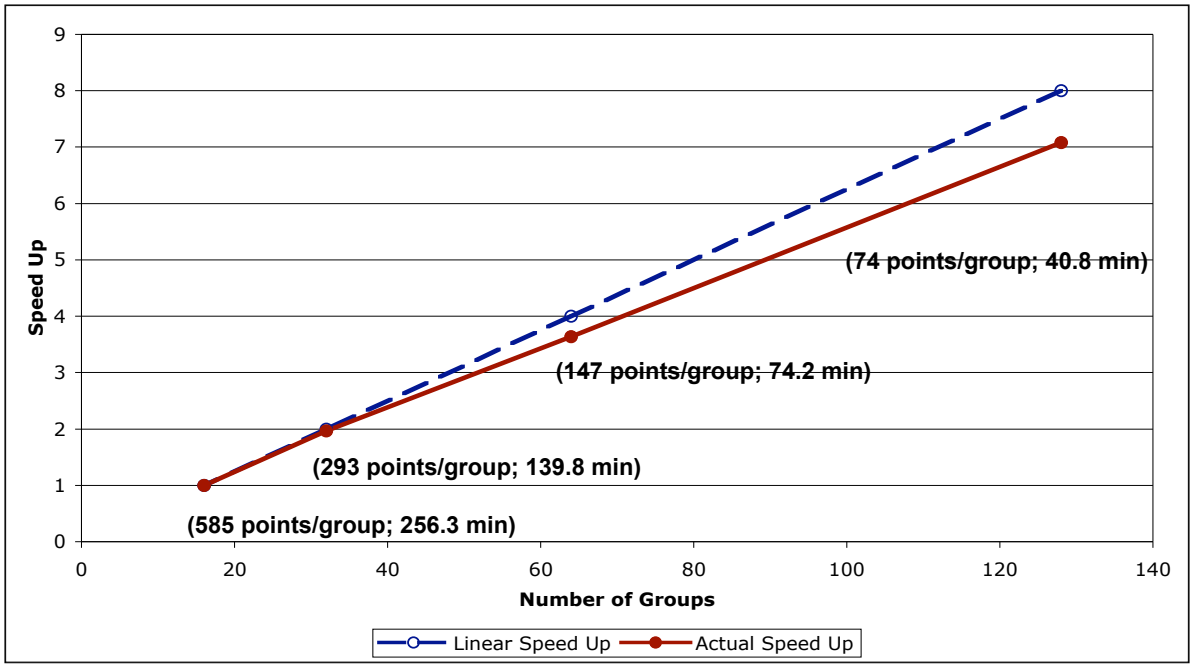

Table 1. MP2 and CCSD H_3^+ diagonal frequencies with the cc-pVDZ (ccd), cc-pVTZ (cct), and cc-pVQZ (ccq) basis sets. The amplitude (amp=n_i) maps onto the energy level (n_i=0,1,2,…), see text. Increasing the value of amp corresponds to a larger spacing of the PES points along the normal mode.

MP2/ccd	harm	amp=1	amp=2	amp=3	amp=4	amp=5	amp=6	amp=7
ν_1	3591	4153	3614	3509	3489	3486	**3486**	3486
ν_2	2712	3152	2812	2779	2777	**2777**	2777	2777
ν_3	2712	3156	2833	2811	**2811**	2811	2811	2811
MP2/cct	harm	amp=1	amp=2	amp=3	amp=4	amp=5	amp=6	amp=7
ν_1	3481	4033	3512	3410	3391	3388	**3388**	3388
ν_2	2813	3266	2913	2880	2878	**2878**	2878	2878
ν_3	2813	3269	2930	2905	**2905**	2905	2905	2905
CCSD/ccd	harm	amp=1	amp=2	amp=3	amp=4	amp=5	amp=6	amp=7
ν_1	3546	4101	3568	3463	3443	3440	**3440**	3440
ν_2	2666	3101	2776	2749	2748	**2748**	2748	2748
ν_3	2666	3101	2776	2749	2748	**2748**	2748	2748
CCSD/cct	harm	amp=1	amp=2	amp=3	amp=4	amp=5	amp=6	amp=7
ν_1	3432	3976	3462	3360	3340	3337	**3337**	3337
ν_2	2763	3211	2872	2843	2842	**2842**	2842	2842
ν_3	2763	3211	2872	2843	2842	**2842**	2842	2842
CCSD/ccq	harm	amp=1	amp=2	amp=3	amp=4	amp=5	amp=6	amp=7
ν_1	3436	3980	3464	3361	3342	3339	3338	**3338**
ν_2	2772	3220	2879	2850	2849	**2849**	2849	2849
ν_3	2771	3220	2879	2850	2849	**2849**	2849	2849

ν_1 - ring breathing, a'
ν_2 and ν_3 - ring deformation, e'

Table 2. H_3^+. MP2 and CCSD calculations with the cc-pVDZ (ccd), cc-pVTZ (cct), and cc-pVQZ (ccq) basis sets. The actual values of harmonic (harm), scaled harmonic (harm(scal)), anharmonic in Cartesian coordinates (anhr(cart)), anharmonic in internals using 2 bonds and the angle (anhr(int)2ba), anharmonic in internals using 3 bonds (anhr(int)3b), and experimental[27,28] (exp) values are given.

	mode	harm	harm(scal)	anhr(cart)	anhr(int)3b	anhr(int)2ba	exp
MP2/ccd	ν_1	3591	3411	3322	3299	3317	3178
	ν_2	2712	2577	2485	2544	2395	2521
	ν_3	2712	2577	2360	2509	2714	2521
MP2/cct	ν_1	3481	3258	3234	3215	3247	
	ν_2	2813	2633	2537	2608	2615	
	ν_3	2813	2633	2425	2578	3149	
CCSD/ccd	ν_1	3546	3358	3274	3251	3285	
	ν_2	2666	2524	2380	2478	2640	
	ν_3	2666	2524	2380	2478	2689	
CCSD/cct	ν_1	3432	3230	3182	3162	3160	
	ν_2	2763	2600	2433	2541	2670	
	ν_3	2763	2600	2433	2541	2697	
CCSD/ccq	ν_1	3436		3181	3161	3137	
	ν_2	2772		2440	2546	2647	
	ν_3	2771		2440	2546	2612	
CCSD/cct	$\nu_1\nu_2$	6195	5830	5464	5585		5554
	$2\nu_2$	5526	5200	4363	4989		4998
	$3\nu_2$	8289	7800	6627	7633		7493
CCSD/ccq	$\nu_1\nu_2$	6208		5471	5587		
	$2\nu_2$	5543		4496	4998		
	$3\nu_2$	8315		6687	7644		

ν_1 - ring breathing, a'
ν_2 and ν_3 - ring deformation, e'

Table 3. Experimental frequencies[27,28] and the errors between calculated and experimental frequencies for H_3^+. Calculations were performed at MP2 and CCSD levels of theory with the cc-pVDZ (ccd), cc-pVTZ (cct), and cc-pVQZ (ccq) basis sets. The following frequencies were calculated: harmonic (harm), scaled harmonic (harm(scal)), anharmonic in Cartesian coordinates (anhr(cart)), anharmonic in internal coordinates (anhr(int)).

H_3^+	mode	harm	harm(scal)	anhr(cart)	anhr(int)	exp
MP2/ccd	ν1	413	233	144	121	3178
	ν2	191	55	-36	22	2521
	ν3	191	55	-162	-12	2521
MP2/cct	ν1	303	80	56	37	
	ν2	291	111	16	87	
	ν3	291	111	-96	56	
CCSD/ccd	ν1	367	180	96	73	
	ν2	144	3	-141	-44	
	ν3	144	3	-141	-44	
CCSD/cct	ν1	254	51	3	-16	
	ν2	242	79	-88	20	
	ν3	242	79	-88	20	
CCSD/ccq	ν1	258		3	-17	
	ν2	250		-81	24	
	ν3	250		-81	24	

ν_1 - ring breathing, a'
ν_2 and ν_3 - ring deformation, e'

Table 4. Experimental frequencies[19] and the errors between calculated and experimental frequencies for HNO_2. Calculations were performed with MP2 and CCSD(T) using the cc-pVDZ (ccd), and cc-pVTZ (cct) basis sets. The following frequencies were calculated: harmonic (harm), scaled harmonic (harm(scal)), anharmonic in Cartesian coordinates (anhr(cart)), and anharmonic in internal coordinates (anhr(int)).

	mode	harm	harm(scal)	anhr(cart)	anhr(int)	exp
MP2/ccd	ν1	196	6	-36	33	3591
	ν2	-20	-104	-51	-44	1700
	ν3	36	-29	-46	5	1263
	ν4	63	20	26	31	790
	ν5	29	-3	-3	9	596
	ν6	48	19	-52	15	543
MP2/cct	ν1	200	-42	-39	28	
	ν2	-28	-135	-51	-44	
	ν3	35	-48	-44	11	
	ν4	47	-7	30	36	
	ν5	25	-15	0	10	
	ν6	51	13	-51	19	
CCSD(T)/ccd	ν1	184	105	-56	14	
	ν2	40	3	6	13	
	ν3	53	25	-33	20	
	ν4	47	30	17	23	
	ν5	19	6	-9	2	
	ν6	29	17	-74	-4	
CCSD(T)/cct	ν1	203	108	-31	31	
	ν2	28	-15	-4	2	
	ν3	56	23	-26	25	
	ν4	52	31	24	29	
	ν5	32	16	8	18	
	ν6	31	16	-65	0	

ν_1 - O-H stretch
ν_2 - O4-N3 stretch
ν_3 - H-O-N bend
ν_4 - O2-N3 stretch
ν_5 - O-N-O bend
ν_6 - torsion

Table 5. Calculated anharmonic vibrational frequencies for HNO_2 and HNO_3 at CCSD(T) with the cc-pVDZ basis set. Frequencies were calculated without coupling (diag) or with coupling but only using VSCF level without a PT2 correction (vscf). Depending on the type of coordinates in which the PES was created, diag(cart) and vscf(cart) correspond to Cartesian coordinates, while diag(int) and vscf(int) correspond to internal coordinates. Difference between diag(cart) and vscf(cart) is labeled as diff(cart), while difference in diag(int) and vscf(int) is labeled as diff(int). Difference between diag(cart) and diag(int) is given as diff(diag).

HNO_2							
mode	diag(cart)	vscf(cart)	diag(int)	vscf(int)	diff(cart)	diff(int)	diff(diag)
ν1	3612	3514	3612	3605	**98**	**7**	0
ν2	1718	1709	1717	1714	9	4	0
ν3	1348	1264	1306	1286	**84**	**20**	**42**
ν4	830	812	832	815	19	17	-1
ν5	609	596	606	600	13	6	3
ν6	779	557	552	539	**222**	**13**	**227**
HNO_3							
mode	diag(cart)	vscf(cart)	diag(int)	vscf(int)	Diff(cart)	Diff(int)	Diff(diag)
ν1	3577	3474	3577	3565	**103**	**12**	0
ν2	1809	1755	1811	1765	54	46	-2
ν3	1365	1342	1362	1350	23	13	2
ν4	1363	1299	1349	1321	**64**	**29**	14
ν5	901	883	898	886	18	12	3
ν6	765	751	778	766	14	11	-13
ν7	650	636	651	641	15	10	-1
ν8	584	567	583	576	17	7	1
ν9	752	492	455	449	**260**	**6**	**297**

HNO_2 molecule
ν_1 - O-H stretch
ν_2 - O4-N3 stretch
ν_3 - H-O-N bend
ν_4 - O2-N3 stretch
ν_5 - O-N-O bend
ν_6 - torsion

HNO_3 molecule
ν_1 - O-H stretch
ν_2 - O4-N1 and O3-N1 ass stretch
ν_3 - O4-N1 and O3-N1 sym stretch
ν_4 - H-O-N bend
ν_5 - O2-N1 stretch
ν_6 - N out of the plane motion
ν_7 - O4-N1-O3 bend
ν_8 - O3-N1-O2 bend
ν_9 - H5-O2-N1-O3 torsion

Table 6. Experimental frequencies[19] and the errors between calculated and experimental frequencies for HNO_3. Calculations were performed with MP2 and CCSD(T) and the cc-pVDZ (ccd), and cc-pVTZ (cct) basis sets. The following frequencies were calculated: harmonic (harm), scaled harmonic (harm(scal)), anharmonic in Cartesian coordinates (anhr(cart)), and anharmonic in internal coordinates (anhr(int)).

	mode	harm	harm(scal)	anhr(cart)	anhr(int)	exp
MP2/ccd	ν1	199	11	-30	30	3550
	ν2	203	107	177	186	1708
	ν3	27	-41	-1	13	1331
	ν4	26	-41	-40	1	1325
	ν5	28	-17	7	9	879
	ν6	12	-27	1	15	762
	ν7	19	-14	3	9	647
	ν8	9	-20	-9	6	579
	ν9	36	11	-57	7	456
MP2/cct	ν1	200	-40	-28	33	
	ν2	165	45	139	148	
	ν3	20	-67	-60	-4	
	ν4	9	-76	-13	-5	
	ν5	31	-28	8	11	
	ν6	21	-30	9	23	
	ν7	25	-18	11	16	
	ν8	14	-24	-4	11	
	ν9	42	10	-49	13	
CCSD(T)/ccd	ν1	192	113	-46	14	
	ν2	87	50	39	51	
	ν3	35	6	-3	10	
	ν4	21	-7	-47	-8	
	ν5	22	3	0	4	
	ν6	3	-13	-11	2	
	ν7	4	-10	-14	-9	
	ν8	2	-10	-19	-4	
	ν9	31	21	-75	-8	

CHAPTER 4. REACTION MECHANISM OF THE DIRECT GAS PHASE SYNTHESIS OF H_2O_2 CATALYSED BY Au_3

Bosiljka Njegic and Mark S. Gordon

Abstract

The gas phase reaction of molecular oxygen and hydrogen catalyzed by an Au_3 cluster to yield H_2O_2 was investigated theoretically using second order Z-averaged perturbation theory (ZAPT), with the final energies obtained with the fully size extensive completely renormalized CR-CC(2,3) coupled cluster theory. The proposed reaction mechanism is initiated by adsorption and activation of O_2 on the Au_3 cluster. Molecular hydrogen then binds to the Au_3O_2 global minimum without an energy barrier. The reaction between the activated oxygen and hydrogen molecules proceeds through formation of hydroperoxide (HO_2) and a hydrogen atom, which subsequently react to form the product hydrogen peroxide. All reactants, intermediates and product remain bound to the gold cluster throughout the course of the reaction. The steps in the proposed reaction mechanism have low activation energy barriers below 15 kcal/mol. The overall reaction is highly exothermic by ~30 kcal/mol.

Introduction

Propylene oxide is an important bulk chemical used for production of mainly polyether polyols, propylene glycol and glycol ethers. Thus, manufacturing of

propylene oxide is a very important industrial process, currently mainly achieved by the oxidation of propylene using chlorohydrin or hydrogen peroxide methods[1]. Chlorohydration involves oxidation of propylene by chlorine in the presence of lime and leads to the production of chlorinated organic by-products that are pollutants and as such difficult to dispose of properly. In addition, huge quantities of $CaCl_2$ are produced that do not have any practical use, but also need to be disposed of. On the other hand, hydrogen peroxide processes are carried out using organic peroxides, mainly derived from isobutene and ethylbenzene, which yield useful co-products, such as *t*-butanol (a gasoline additive) and 1-phenyl ethanol that can be dehydrated to styrene and subsequently polymerized into the important synthetic material polystyrene. However, epoxide production by this approach is not yet cost effective.

Hydrogen peroxide might be a natural choice of oxidant for the epoxidation of propene; however, an effective catalyst is needed. Although the catalytic activity of gold was recognized as early as the 1980's[2] an important breakthrough came through the work of Haruta *et al.*[3] in the mid 1990's. These authors demonstrated that gold nanoparticles supported on titanium silicates catalyze the epoxidation of propene by hydrogen peroxide species formed *in situ* from gaseous hydrogen and oxygen. Recently several companies have developed a new approach[4] in which hydrogen peroxide is used as an oxidant, thus making the production of propylene oxide a green industrial process since the by-product is water.

A very nice review on the epoxidation of propene by Min and Friend[5] also noted that although the propene epoxidation mechanism is still under investigation, a hydrogen peroxo-like species is the likely oxidant. This assertion is supported by the

known effective epoxidation of propene by hydrogen peroxide promoted by titania catalysts[6]. Furthermore, it has been confirmed experimentally that hydrogen peroxide[7,8] and peroxide species[9] are formed from H_2 and O_2 in the reaction catalyzed by gold supported on titania. However, there is as yet no experimental evidence for the existence of peroxide species during the epoxidation reaction involving H_2 and O_2. An issue that is related to the mechanism of hydrogen peroxide formation from H_2 and O_2 over gold catalysts is that hydrogen peroxide production currently takes place through sequential hydrogenation and oxidation of an alkyl anthraquinone[1]. This method is limited by the cost of the solvent, the necessity of periodic replacement of the catalyst due to hydrogenation, and the large scale of the production. This last point further increases the cost because of the risks related to transportation and storage of the produced hydrogen peroxide.

A recent study by Weckhuysen et al.[10] suggests a possible explanation for the aforementioned lack of experimental evidence for peroxide. According to their proposed mechanism, the reaction proceeds though the binding of propene to titania to produce a propoxy species, which then gets desorbed from the catalyst by a peroxide species to form epoxide and water. If the formation of the peroxide species is indeed the rate-controlling step of the epoxidation reaction, then one may infer that the concentration of this intermediate will stay below the sensitivity of detection throughout the reaction. However, a theoretical study[11] carried out with density functional theory (DFT) suggests that the epoxidation of propene is the rate controlling step, with an activation energy of 19.6 kcal/mol, while formation of the peroxide species requires only 2.2 kcal/mol. Therefore, further theoretical work is

needed to help resolve the discrepancy between experimental data and theoretical predictions.

The intent of the work presented in this paper is to shed additional light on the mechanism of the H_2/O_2 reaction catalyzed by an Au_3 cluster to form an intermediate hydroperoxide, a possible oxidant in the epoxidation reaction, and the final product, hydrogen peroxide, an important oxidant under mild conditions. The size of the gold cluster was chosen based on two factors. The number of gold atoms needs to be reasonably small, so accurate *ab initio* calculations, such as perturbation theory and coupled cluster theory, can be employed. On the other hand, the gold cluster needs to be large enough to bind both O_2, which prefers to bind to clusters with an odd number of electrons[12,13], and H_2, which does not bind to negatively charged clusters[14]. Hence, Au_3 is the simplest useful gold cluster to model H_2O_2 formation. Activation energy barriers and the overall reaction enthalpy are reported.

Computational Details

Geometry and saddle point optimizations[15-17], Hessians (energy second derivatives)[18,19] and intrinsic reaction paths[20-24] are calculated with (spin-correct) Z-averaged second order perturbation theory (ZAPT)[25,26]. All stationary points are tightly optimized, with the largest component of the analytic gradient[27,28] being smaller than 10^{-5} Hartree/Bohr. Hessian calculations were obtained semi-numerically using double differencing of analytic gradients.

The general approach used for locating transition states was to create a linear least motion path (LLM), determined by linear interpolation between the coordinates of the two corresponding minima. Single point energy calculations were performed at each LLM point. This was followed by constrained optimizations at each of these points, thereby creating a linear synchronous transit (LST) path. The structure with the highest energy on the LST path is then chosen as the starting point for locating the transition state. The optimized geometries for all stationary points were used to do single point energy calculations with restricted open shell completely renormalized left eigenvalue singles and doubles coupled cluster theory with perturbative triples, CR-CCSD(T)$_L$[29,30]. The CR-CCSD(T)$_L$ (or, equivalently CR-CC(2,3)) method is size extensive and has been shown to break single bonds correctly for both open and closed shell species[31] The shorthand notation used here for this method is CCL. These CCL energies were then used to calculate more accurate energy barriers (ΔE_b) and activation energies (ΔE_a), which include zero point energy (ZPE) corrections, calculated with the harmonic approximation without frequency scaling, and thermal corrections to 425K. The latter temperature was chosen based on the experimental conditions for the epoxidation reaction[32]. The apparent energy of activation (ΔE_a(app)) is calculated as the difference in the energy of the highest transition state and the reactants. Binding energies (ΔE_{bind}) are calculated as the difference between the energy of the product and the sum of the energies of the separated species. The reaction enthalpy (ΔH_r) represents the difference in the enthalpies of the product and reactants.

The effective core potential (ECP) with scalar relativistic corrections (SBKJC)[33] augmented by one set of *f* polarization functions (exponent=0.89) and one *s* and one set of p diffuse functions (exponent=0.01) were used on gold atoms, with the $5s^2 5p^6 5d^{10} 6s^1$ electrons treated explicitly. Oxygen and hydrogen atoms employed the 6-31++G(d,p) basis set[34]. Spherical harmonic basis functions were used. The GAMESS (General Atomic and Molecular Electronic Structure System) program suite[35,36] was used in all the calculations and molecules were visualized with MacMolPlt[37].

Results and Discussion

The optimized structures and highest occupied molecular orbitals of Au_3, H_2O_2, O_2 and H_2 are shown in Figure 1. The Au_3 global minimum has C_{2v} symmetry with a $^2B_2$ ground state, in accordance with experiment[38]. The three Au_3 molecular orbitals (MO) that arise from linear combinations of Au 6s atomic orbitals are also illustrated in Figure 1. These are the bonding HOMO (highest occupied MO), the non-bonding SOMO (singly occupied MO) and the LUMO (lowest unoccupied MO). The O_2 $D_{\infty h}$ ground term is $^3\Sigma_g^-$. This term corresponds to $^3B_{1g}$ in D_{2h}, which was used in the calculations.

The minima located on the Au_3O_2 potential energy surface (PES) are reported in Figure 2. There are two possible ways in which O_2 can bind to Au_3. One is an "end-on" structure in which binding occurs through one oxygen and one gold atom. This structure belongs to C_s symmetry and both terms $^2A'$ (Figure 2a) and $^2A''$ (Figure 2b) were found, with $^2A''$ being lower in energy. O_2 can also bind in a bridging

manner. In this C_{2v} arrangement, two oxygen atoms bind to two gold atoms forming a four-member ring. Three bridging minima, corresponding to $^2A_1$ (Figure 2c), $^2B_2$ (Figure 2d) and $^2A_2$ (Figure 2e), have been found, with $^2A_2$ being the ground state term. The predicted global minimum with O_2 bridging between two Au atoms is in accordance with most recent published theoretical work[11,12], while older studies reported the end-on structure to be the global minimum[13,39,40]. Some studies used the end-on species as the reactant rather than the global minimum bridging structure[41].

Table 1 lists binding energies at 0K with and without ZPE corrections. The latter makes a small contribution in most cases. The ZAPT level of theory predicts that O_2 binds to Au_3 with a binding energy of ~8.5 kcal/mol, while the CCL binding energy is a much larger 14.5 kcal/mol. Previous DFT studies predict Au_3-O_2 binding energies of 7[11], 5.8-16.1[39], 15.2[40], and 20.8 kcal/mol[12]. All of these calculations predict that O_2 will bind to Au_3. It is likely that CCL provides the most accurate prediction.

Now, consider the Au_3 - O_2 interaction in greater detail. O_2 is a ground state triplet diradical with two degenerate singly occupied π^* orbitals. In C_{2v} symmetry these two π^* orbitals of O_2 exhibit b_2 and a_2 symmetry. Au_3 has an unpaired electron located in the σ nonbonding orbital with b_2 symmetry (see Figure 1). Binding of O_2 to Au_3 occurs by the pairing of the unpaired electron in the Au_3 b_2 orbital with an unpaired electron in the O_2 π^* b_2 orbital. This leads to the formation of the Au_3O_2

global minimum, leaving the remaining unpaired electron in the a_2 π^* orbital, yielding the ground state term.

Starting from the Au_3O_2 global minimum, H_2 was positioned ~ 5 Å away, and geometry optimization was performed in C_s symmetry. No intervening barrier was found to prevent the binding of H_2 to Au_3O_2 to form $H_2Au_3O_2$. The latter species is the starting structure (reactant) presented as the first minimum (Min1, the first point along the x-axis) in Figure 3. This figure depicts the reaction coordinate diagram for the formation of H_2O_2 catalyzed by Au_3. As reported in Table 1, at the ZAPT level of theory, H_2 binds to Au_3 by 7.5 (4.7) without (with) the ZPE correction. The CCL binding energy, in contrast, is very small. Indeed CCL with the ZPE correction predicts the addition of H_2 to Au_3O_2 to be slightly endothermic. Since the structures were not optimized at the coupled cluster level of theory and since anharmonicity and coupling of the vibrations were not taken into account, the addition of H_2 to Au_3O_2 could be either weakly exothermic or weakly endothermic.

Now consider (Figure 3) the ZAPT reaction mechanism at 0K, disregarding ZPE and thermal corrections. The starting structure (Figure 3, Min1) has both O_2 and H_2 bound to the Au_3 cluster. The reaction starts by breaking the H-H bond and transferring the first hydrogen atom to O_2 to form a hydroperoxide intermediate. This step, which proceeds in C_s symmetry, must surmount a 9.4 kcal/mol barrier.

The attempt to locate the next transition structure (Figure 3, TS2-3) was unsuccessful, due to convergence problems in this region of the restricted open shell Hartree Fock (ROHF)/ZAPT potential energy surface, possibly due to some configurational mixing. Thus, points along the ZAPT LLM path were employed to

simulate this part of the reaction path, and the point with the highest energy on the LLM path is taken to be the approximate TS for this step. The corresponding energy "barrier" of 3.5 kcal/mol is an upper limit to the actual barrier at the true transition state. Based on this small barrier, there may be some residual weak binding between the HO_2 hydrogen and the adjacent gold atom. On the other hand, CCL single points along this path suggest that there is no barrier at all in this region (i.e., TS2-3) of the reaction path.

The next two steps on the reaction path involve rearrangements of the HO_2 species, in order to attain an arrangement that is convenient for the ultimate formation of H_2O_2. These two steps proceed through ZAPT barriers of 9.1 (Figure 3, TS3-4) and 2.2 (Figure 3, TS4-5) kcal/mol. The second hydrogen atom then undergoes a 1,2-shift from one Au atom to form an Au-H-Au bridge. The ZAPT barrier for this step (Figure 3, TS5-6) is 7.9 kcal/mol. This is followed by a repositioning of HO_2 with a small ≤2.4 kcal/mol barrier (Figure 3, TS6-7), determined by following the corresponding LLM path.

The last two steps on the reaction path involve the completion of the transfer of the bridging H to the Au atom on which the HO_2 moiety resides, with a relatively low barrier of 4.6 kcal/mol (Figure 3, TS7-8), and then the formation of H_2O_2 via a 7.6 kcal/mol barrier (Figure 3, TS8-9).

The ZAPT and CCL reaction paths shown in Figure 3 are in qualitative agreement with each other. These findings may be compared with a previous DFT study[11], which reports a very small 2.2 kcal barrier for the formation of HO_2, and a 15.1 kcal/mol barrier for H_2O_2 formation. This DFT study also predicts that the rate-

controlling step in the epoxidation reaction is the actual epoxidation of propene with an activation barrier of 19.6 kcal/mol, rather than the formation of the hydroperoxide intermediate. A DFT study on the formation of H_2O_2 from H_2 and O_2 over Au_3[41], predicts the desorption of H_2O_2 to be the rate-controlling step with a barrier of 8.6 kcal/mol. So, the DFT predicted highest point on the reaction path shown in Figure 3 is roughly half that predicted by CCL, presumably the most reliable level of theory.

The calculated activation energies (ΔE_a) and apparent energies of activation (ΔE_a(app)) are listed in Table 2. The rate-controlling step is the last step of the reaction that leads to the formation of H_2O_2. The most accurate (CCL) calculation gives ΔE_a(app)=14.0 kcal/mol with both ZPE and thermal corrections at 425K included. Note also that a CCL activation energy of almost 7 kcal/mol is needed for the formation of HO_2. The most accurate (CCL) calculation predicts ΔH_r(425K)=-27.6 kcal/mol. Inclusion of ZPE decreases, while the thermal correction increases the amount of released energy.

Selected minima are shown in Figure 4 with emphasis on some geometrical parameters of interest and on the highest singly occupied molecular orbital. Bond lengths and angles are chosen to illustrate important changes throughout the course of the reaction. Atoms are labeled and numbered as shown on the first structure.

It is informative to follow the electron density distribution of the unpaired electron, as depicted in Figure 4 using Mulliken populations in the singly occupied orbitals. The reaction starts with the unpaired electron on Au_3 and a pair of unpaired electrons on O_2. Upon binding of O_2 to Au_3, the unpaired electron localizes mostly in the pair of O_2 π^* orbitals, as shown by the Mulliken spin populations of ~0.5 on each

of the oxygen atoms (Figure 4a). As the reaction progresses this electron density becomes somewhat delocalized, as shown in the spin populations on Min4 in Figure 4b. Here, electron density is distributed among mostly gold atoms, which have atomic spin population ranging from 0.17 to 0.34. Somewhat lower Mulliken populations are found on the two H (~0.1) and two O (~0.1) atoms (Figure 4b). However, in the product the unpaired electron density localizes in the nonbonding Au_3 σ orbital, with atomic spin populations of ~0.45 on both Au6 and Au7 (Figure 4c). This Au_3 orbital is involved in the binding of O_2 to Au_3, so the catalytic cycle can proceed through the binding of the next O_2 molecule and simultaneous desorption of the formed H_2O_2 from Au_3 (Figure 4d).

Conclusions

A reaction mechanism for gas phase formation of H_2O_2 from H_2 and O_2 catalyzed by Au_3 is proposed. The catalytic activity of gold is achieved by activation of both O_2 and H_2 by weakening the O-O and H-H bonds. In addition, transfer of two hydrogen atoms to form first HO_2 radical and subsequently the molecule H_2O_2, are realized in a cascade of steps, each having a relatively low energy of activation. The most accurate calculations with ZPE and thermal corrections at 425K included, predict the final step of the reaction to be rate controlling. The apparent energy of activation is 14.0 kcal/mol, although it is important to note that the formation of HO_2 does require overcoming a barrier of almost 7 kcal/mol. The reaction is predicted to be highly exothermic by 27.6 kcal/mol.

Acknowledgments

This work was supported by grants from the Air Force Office of Scientific Research. The authors are grateful to Drs. Michael Schmidt and Ryan Olson, and to Professor Takako Kudo enlightening discussions.

References

(1) *Kirk-Othmer concise encyclopedia of chemical technology*, 5th ed.; Wiley-Interscience: Hoboken, N.J., 2007.

(2) Haruta, M.; Kobayashi, T.; Sano, H.; Yamada, N. *Chemistry Letters* **1987**, 405.

(3) Kalvachev, Y. A.; Hayashi, T.; Tsubota, S.; Haruta, M. *Studies in Surface Science and Catalysis* **1997**, *110*, 965.

(4) *http://www.corporate.basf.com/en/investor/news/mitteilungen/pm.htm?pmid=2444&id=6ZLRUBxn_bcp.4k*, 2006.

(5) Min Byoung, K.; Friend Cynthia, M. *Chemical reviews* **2007**, *107*, 2709.

(6) Clerici, M. G.; Bellussi, G.; Romano, U. *Journal of Catalysis* **1991**, *129*, 159.

(7) Landon, P.; Collier Paul, J.; Papworth Adam, J.; Kiely Christopher, J.; Hutchings Graham, J. *Chemical communications (Cambridge, England)* **2002**, 2058.

(8) Okumura, M.; Kitagawa, Y.; Yamagcuhi, K.; Akita, T.; Tsubota, S.; Haruta, M. *Chemistry Letters* **2003**, *32*, 822.

(9) Sivadinarayana, C.; Choudhary, T. V.; Daemen, L. L.; Eckert, J.; Goodman, D. W. *Journal of the American Chemical Society* **2004**, *126*, 38.

(10) Nijhuis, T. A.; Gardner, T. Q.; Weckhuysen, B. M. *Journal of Catalysis* **2005**, *236*, 153.

(11) Joshi, A. M.; Delgass, W. N.; Thomson, K. T. *Journal of Physical Chemistry B* **2006**, *110*, 2572.

(12) Mills, G.; Gordon, M. S.; Metiu, H. *Chemical Physics Letters* **2002**, *359*, 493.

(13) Varganov, S. A.; Olson, R. M.; Gordon, M. S.; Metiu, H. *Journal of Chemical Physics* **2003**, *119*, 2531.

(14) Varganov, S. A.; Olson, R. M.; Gordon, M. S.; Mills, G.; Metiu, H. *Journal of Chemical Physics* **2004**, *120*, 5169.

(15) Baker, J. *Journal of Computational Chemistry* **1986**, *7*, 385.

(16) Culot, P.; Dive, G.; Nguyen, V. H.; Ghuysen, J. M. *Theoretica Chimica Acta* **1992**, *82*, 189.

(17) Helgaker, T. *Chemical Physics Letters* **1991**, *182*, 503.

(18) Takada, T.; Dupuis, M.; King, H. F. *Journal of Chemical Physics* **1981**, *75*, 332.

(19) Gwinn, W. D. *Journal of Chemical Physics* **1971**, *55*, 477.

(20) Gonzalez, C.; Schlegel, H. B. *Journal of Chemical Physics* **1989**, *90*, 2154.

(21) Schmidt, M. W.; Gordon, M. S.; Dupuis, M. *Journal of the American Chemical Society* **1985**, *107*, 2585.

(22) Ishida, K.; Morokuma, K.; Komornicki, A. *Journal of Chemical Physics* **1977**, *66*, 2153.

(23) Baldridge, K. K.; Gordon, M. S.; Steckler, R.; Truhlar, D. G. *Journal of Physical Chemistry* **1989**, *93*, 5107.

(24) Garrett, B. C.; Redmon, M. J.; Steckler, R.; Truhlar, D. G.; Baldridge, K. K.; Bartol, D.; Schmidt, M. W.; Gordon, M. S. *Journal of Physical Chemistry* **1988**, *92*, 1476.

(25) Lee, T. J.; Rendell, A. P.; Dyall, K. G.; Jayatilaka, D. *Journal of Chemical Physics* **1994**, *100*, 7400.

(26) Lee, T. J.; Jayatilaka, D. *Chemical Physics Letters* **1993**, *201*, 1.

(27) Fletcher, G. D.; Gordon, M. S.; Bell, R. S. *Theoretical Chemistry Accounts* **2002**, *107*, 57.

(28) Aikens, C. M.; Fletcher, G. D.; Schmidt, M. W.; Gordon, M. S. *Journal of Chemical Physics* **2006**, *124*, 014107/1.

(29) Wloch, M.; Gour, J. R.; Piecuch, P. *Journal of Physical Chemistry A* **2007**, *111*, 11359.

(30) Piecuch, P.; Wloch, M. *The Journal of chemical physics* **2005**, *123*, 224105.

(31) Ge, Y.; Gordon, M. S.; Piecuch, P. *Journal of Chemical Physics* **2007**, *127*, 174106/1.

(32) Sinha, A. K.; Seelan, S.; Okumura, M.; Akita, T.; Tsubota, S.; Haruta, M. *Journal of Physical Chemistry B* **2005**, *109*, 3956.

(33) Stevens, W. J.; Krauss, M.; Basch, H.; Jasien, P. G. *Canadian Journal of Chemistry* **1992**, *70*, 612.

(34) Hehre, W. J.; Ditchfield, R.; Pople, J. A. *Journal of Chemical Physics* **1972**, *56*, 2257.

(35) Schmidt, M. W.; Baldridge, K. K.; Boatz, J. A.; Elbert, S. T.; Gordon, M. S.; Jensen, J. H.; Koseki, S.; Matsunaga, N.; Nguyen, K. A.; et al. *Journal of Computational Chemistry* **1993**, *14*, 1347.

(36) Gordon, M. S.; Schmidt, M. W. *Theory and Applications of Computational Chemistry: The First Forty Years* **2005**, 1167.

(37) Bode, B. M.; Gordon, M. S. *Journal of Molecular Graphics & Modelling* **1998**, *16*, 133.

(38) Howard, J. A.; Sutcliffe, R.; Mile, B. *Journal of the Chemical Society, Chemical Communications* **1983**, 1449.

(39) Ding, X.; Li, Z.; Yang, J.; Hou, J. G.; Zhu, Q. *Journal of Chemical Physics* **2004**, *120*, 9594.

(40) Yoon, B.; Haekkinen, H.; Landman, U. *Journal of Physical Chemistry A* **2003**, *107*, 4066.

(41) Wells, D. H.; Delgass, W. N.; Thomson, K. T. *Journal of Catalysis* **2004**, *225*, 69.

(42) Russell, D. J. I. *NIST Computational Chemistry Comparison and Benchmark Database, NIST Standard Reference Database Number 101*, 2005.

Figure 1. ZAPT optimized geometries of a.) Au_3, b.) O_2, c.) H_2, and d.) H_2O_2. The $^3\Sigma_g^-$ in $D_{\infty h}$ corresponds to $^3B_{1g}$ in D_{2h} for O_2. On the right of the structures all three σ orbitals are shown for Au_3, and for the rest of the molecules the highest occupied orbitals are shown. Experimental data[42] are given in parentheses.

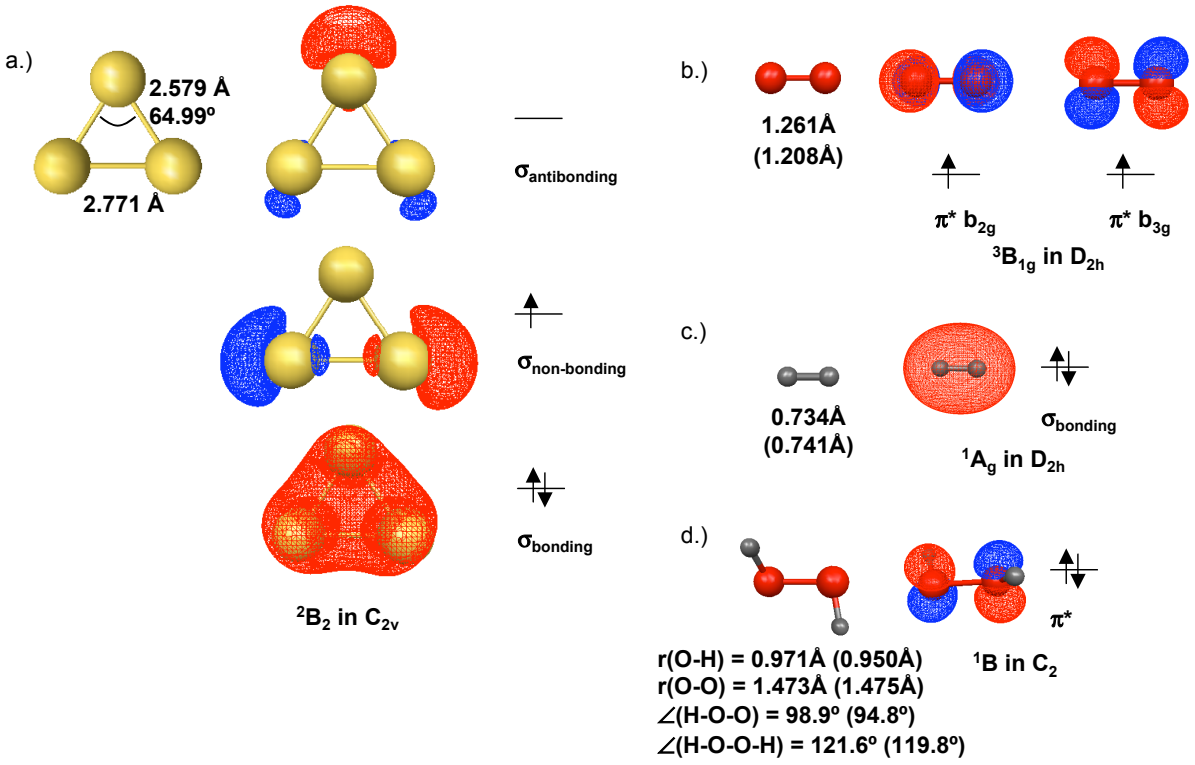

Figure 2. ZAPT geometries of O_2 bound to Au_3 in C_s symmetry. The geometric parameters are given on the left, while the term and corresponding highest single occupied orbital are given on the right, with the relative energy with respect to the energy of separate species, $Au_3 + O_2$.

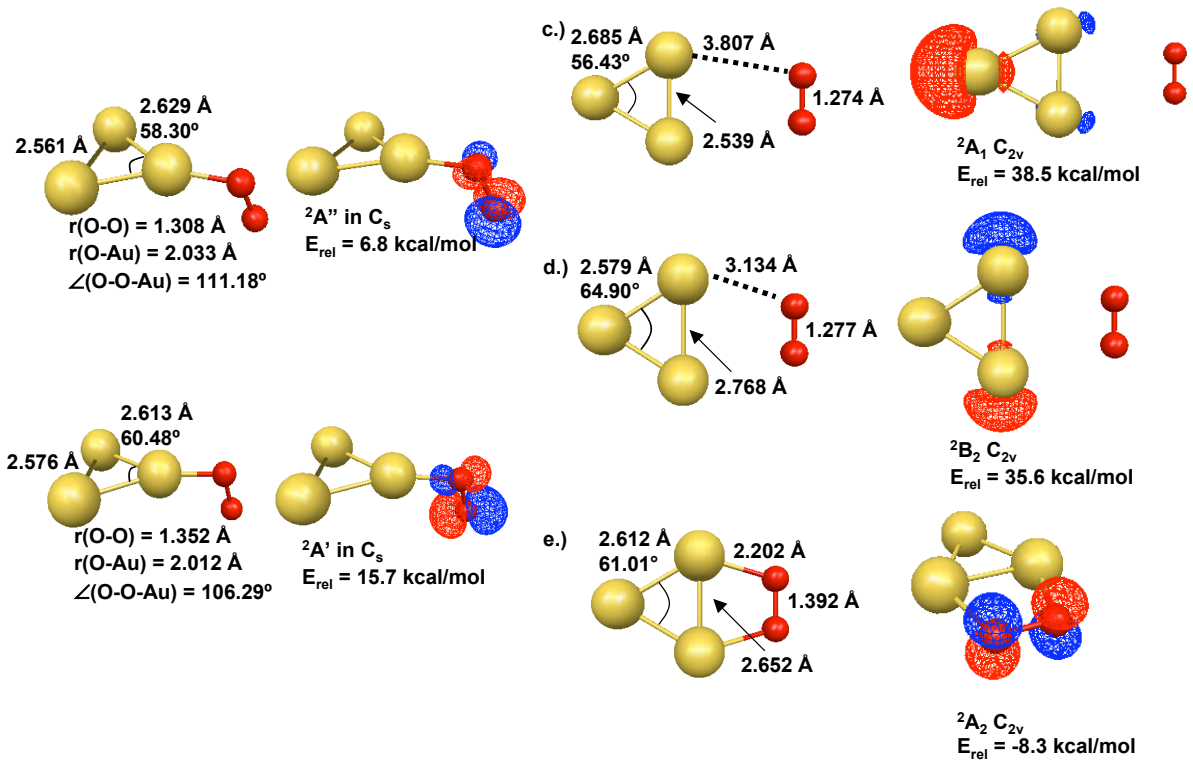

Figure 3. Reaction coordinate diagram of H_2O_2 formation from gaseous molecular O_2 and H_2 catalyzed by Au_3. Minima (Min) are given below the reaction curve, while transition states(TS) are pictured above it. The corresponding imaginary frequency is given below each TS geometry, followed by the ZAPT energy barrier and the CCL energy barrier (in parentheses), in kcal/mol. The ZAPT and CCL apparent energy barriers (ΔE_b(app)) and reaction energies (ΔE_r) are also provided, while activation energies and reaction enthalpies at 0K are given in parentheses.

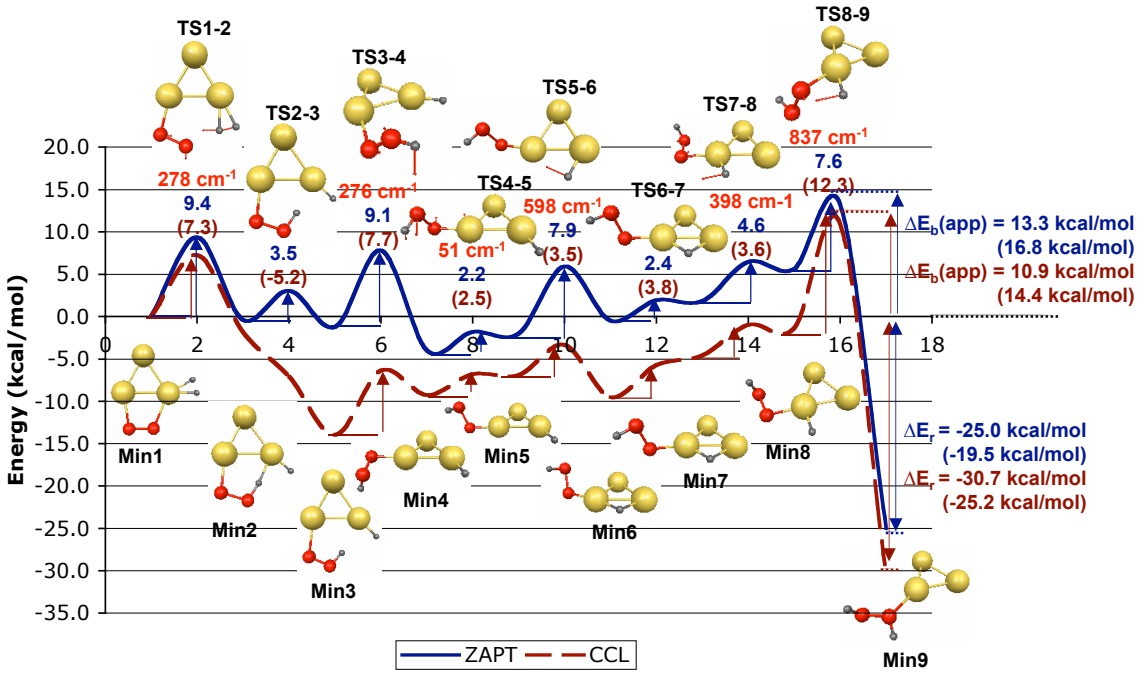

Figure 4. Depicted are the highest occupied orbital and some geometrical parameters. a.)-c.) Selected minima with the same numberings as in Figure 3; the Mulliken atomic spin population is give on the right of the structures. d.) Minimum obtained upon binding of the second O_2 molecule to already formed $Au_3H_2O_2$. Atoms are numbered as shown on the first structure.

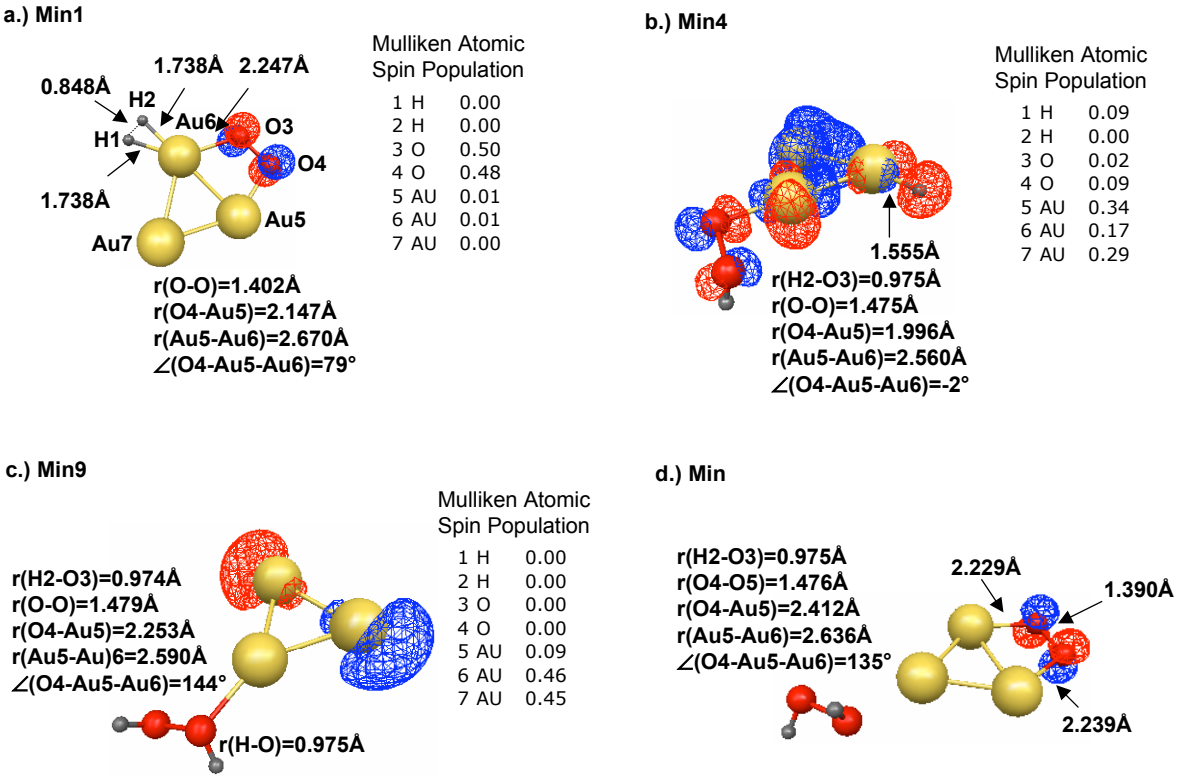

Table 1. ZAPT and CCL binding energies (ΔE_{bind}) at 0K, with and without ZPE corrections. Negative values indicate binding.

Binding of	ΔE_{bind} (kcal/mol)			
	ZAPT	ZAPT+ZPE	CCL	CCL+ZPE
O_2 to Au_3	-8.3	-8.5	-14.5	-14.7
H_2 to Au_3O_2	-7.5	-4.7	-1.7	1.0
H_2O_2 to Au_3	-15.6	-15.7	-12.9	-13.0
O_2 to $Au_3H_2O_2$	-2.6	-1.8		

Table 2. ZAPT and CCL activation energies (ΔE_a), at 0K and 475K, for each forward step of the reaction (see Figure 3). TS(2) and TS(6), correspond to transition states that were estimated rather then located, so no Hessians are available at these points. The apparent energy of activation (ΔE_b(app)) and reaction enthalpy (ΔH_r) are reported as well.

Structure	ΔE_a(ZAPT) (0K)	ΔE_a(ZAPT) (425K)	ΔE_a(CCL) (0K)	ΔE_a(CCL) (425K)
TS(1)	9.2	8.9	7.2	6.8
TS(3)	8.2	8.4	6.8	6.9
TS(4)	0.2	-0.3	0.5	0.0
TS(5)	6.5	6.5	2.1	2.1
TS(7)	4.5	4.0	3.5	3.0
TS(8)	8.4	8.0	13.1	12.7
ΔE_a(app) (kcal/mol)	16.8	16.3	14.4	14.0
ΔH_r (kcal/mol)	-19.5	-21.9	-25.2	-27.6

CHAPTER 5. GENERAL CONCLUSIONS

"… scientific work must not be considered from the point of view of the direct usefulness of it. It must be done for itself, for the beauty of science…"

- Marie Curie (1867–1934)

Summary

The work in this thesis involved explorations of potential energy surfaces to gain an insight into two major problems: calculating accurate vibrational frequencies and deciphering reaction mechanisms.

Chapters 2 and 3 of this thesis were concerned with further development of the Vibrational Self-Consistent Field (VSCF) method. There are two parts of the VSCF method: generating a potential energy surface (PES) on a grid and solving for the vibrational energy levels. Improvements were made in the manner in which the PES is generated. In the standard implementation of the VSCF method, following normal mode displacement vectors in Cartesian coordinates generates the PES. However, it was shown, in Chapters 2 and 3, that following normal mode displacement vectors in internal coordinates creates a PES that yields anharmonic vibrational frequencies of higher accuracy. Furthermore, the spacing of the PES grid points is made flexible, again ensuring the highest accuracy of the calculated frequencies (Chapter 3). Finally, the coarse-grained parallelization of the PES (Chapter 3) was successfully implemented into the GAMESS program suite, thereby enabling VSCF computations on larger systems.

Chapter 4 reports the reaction mechanism of the direct gas phase synthesis of H_2O_2 catalyzed by an Au_3 cluster. This reaction was studied at the ZAPT level of theory with single point energies carried out at the CCL level of theory. The gold cluster activates the H_2 and O_2 molecules. The reaction proceeds through several intermediates and transition states with relatively low barriers. The rate-controlling step is the very last one, in which H_2O_2 is formed. The apparent energy of activation is found to be 14.0 kcal/mol. The reaction is predicted to be highly exothermic by 27.6 kcal/mol.

Future Directions

While the flexible spacing of the PES points in the VSCF method introduced the idea of an adaptive grid, this procedure is not yet automated, something that could be done with relative ease. Furthermore, using adaptive grids may lower the number of grid points needed to generate a reliable PES. If the displacements taken from the equilibrium geometry are small enough, the same range of displacements can be covered with a smaller number of points without degrading the accuracy of the PES. Parallelization of the VSCF code opened the door to calculations on larger molecules, such as polypeptides or hydrogen bound molecular clusters. In these systems, the number of low frequency modes tends to be significant and since these modes are more likely to exhibit a high degree of anharmonicity. Therefore, creating a PES using internal coordinates will be crucial for the accuracy of calculated frequencies. The next big step should be improving the accuracy of the calculated intensities. There is still considerable room to improve both the harmonic and

anharmonic levels of theory. For example, intensity calculations using a normal mode analysis can be enabled at the CCSD level of theory. In the VSCF method intensities are calculated using only the diagonal potential, with coupling terms neglected. This provides another area for improved accuracy.

For the catalysis project, the formation of H_2O_2 is just the first step in exploring the mechanism of the propene epoxidation over gold nanoparticles. Clearly, the epoxidation mechanism has to be explored. Second, the effect of the size of the cluster on the catalytic activity of gold and the associated mechanism is an important issue. In addition, the effect of the metal oxide support on both H_2O_2 formation and the epoxidation process are important avenues of research. Furthermore, questions regarding catalytic promoters and inhibitors or, for example, the role of trace moisture on the catalytic process still have to be explored.